fractal and fractional

MDPI

Article

Optimal FOPI Error Voltage Control Dead-Time Compensation for PMSM Servo System

Fumin Li [1], Ying Luo [1,*], Xin Luo [1], Pengchong Chen [1] and Yangquan Chen [2]

[1] School of Mechanical Science and Engineering, Huazhong University of Science and Technology, Wuhan 430074, China
[2] School of Engineering, University of California, Merced, CA 95343, USA
* Correspondence: ying.luo@hust.edu.cn

Abstract: This paper proposed a dead-time compensation method with fractional-order proportional integral (FOPI) error voltage control. The disturbance voltages caused by the power devices' dead time and non-ideal switching characteristics are compensated for with the FOPI controller and fed to the reference voltage. In this paper, the actual error voltage is calculated based on the model and actual voltage of the permanent magnet synchronous motor. Considering the parameter error of the permanent magnet synchronous motor and the voltage error caused by the dead-time effect, a FOPI controller is used to calculate the compensation voltage. An improved particle swarm optimization (PSO) algorithm is utilized to design the parameters of the FOPI controller in order to eliminate the dead-time effect, and the optimal fitness function is designed. Compared with other optimization algorithms, the improved PSO algorithm can achieve faster convergence speed in the error voltage controller parameter design. The proposed dead-time compensation method can improve the performance of the current response and eliminate the dead-time effect. This method also eliminates all harmonic disturbances and has a good suppression effect on high-frequency harmonics. The simulation and experimental results show that the dead-time compensation method using optimal FOPI error voltage control makes the current ripple smaller and the response speed faster than that of the traditional optimal integer-order PI control, thus demonstrating the effectiveness and advantages of the proposed method.

Keywords: fractional-order proportional integral (FOPI) controller; dead-time compensation; particle swarm optimization (PSO); voltage source inverter (VSI); permanent magnet synchronous motor (PMSM)

Citation: Li, F.; Luo, Y.; Luo, X.; Chen, P.; Chen, Y. Optimal FOPI Error Voltage Control Dead-Time Compensation for PMSM Servo System. *Fractal Fract.* **2023**, *7*, 274. https://doi.org/10.3390/fractalfract7030274

Academic Editors: Arman Oshnoei and Behnam Mohammadi-Ivatloo

Received: 1 January 2023
Revised: 1 March 2023
Accepted: 10 March 2023
Published: 21 March 2023

1. Introduction

The pulse width modulation (PWM) voltage source inverter (VSI) has been extensively used in permanent magnet synchronous motor drive systems. The dead time should be inserted in switching signals to avoid any shoot-through in the inverter lags of the PWM-VSI system. Because of the dead time of the inverter, there is a voltage drop between the output voltage and the reference voltage. The voltage drop caused by the dead time brings serious problems, such as current distortion and torque pulsation. Especially when the current is nearly zero, the output voltage distortion is more severe. Hence, it is vital to reject the disturbance from the dead time and improve the performance of current trucking.

Practical approaches have been discussed to overcome this problem. These methods can be sorted into three categories: (1) methods based on the modification of the PWM signal; (2) methods based on current harmonics monitoring; (3) methods based on model observation.

In the methods based on the modification of the PWM signal, the pulse width error caused by dead time is compensated for by detecting the current polarity and adjusting

the PWM pulse width. In [1], this voltage error is compensated during the next switching period by modification of a reference voltage, the proposed solution can be used to compensate for the voltage error in multilevel multiphase voltage source inverters, but [1] requires additional hardware, which increases the cost and complexity of the system. If the polarity information is not accurate enough, the performance will worsen after compensating. The modified PWM signals are obtained using an off-line calculation in [2], this method relies on the precise detection of current polarity. However, obtaining accurate current polarity at zero-crossing instants is difficult, so it is necessary to determine the current polarity with the help of a more complicated signal processing algorithm. In [3], polarity detection accuracy is improved by using feedback circuits to measure inverter output voltages and Kalman filters to reconstruct fundamental phase currents. These approaches require additional circuits, which increase the end-product cost and hardware complexity.

In the PWM VSI system, the dead-time effect produces sixth-order current harmonics in the synchronous reference frame. According to this theory, the methods based on current harmonic monitoring are proposed [4–11]. The scheme in [4–11] can directly reduce the dead-time current harmonics by generating compensation voltage references while the motor is operating under steady conditions. Although those methods can make the proposed scheme effective in both the steady and transient states, the algorithm converging speed could be improved by limiting computation efforts. In [12], those approaches to the motor design improved the sinusoidal degree of the back electromotive force (EMF) by optimizing the distribution of the stator windings and the structure of the stator slots. Although the approaches can attenuate the harmonics caused by the slot effect and the magnetic saturation, the harmonics generated with the nonlinear characteristics of the inverter still exist [12]. The method based on the proportional-resonant (PR) regulator was also presented. It can track the reference for the positive and negative sequence currents without errors simultaneously [13], although the methods are effective, the interference between the different frequencies needs to be eliminated, and the algorithms need to be simplified. In [4], a dead-time-related harmonic minimization method is proposed based on proportional-integral (PI) controller tuning and under the premise of keeping the same control strategy; however, this method cannot completely eliminate the dead-time effect, which still has a great impact on the control system. This method [4] is compared with the method proposed in this paper. The methods based on current harmonics monitoring cannot take into account the high-frequency harmonic disturbance caused by the dead-time effect; moreover, the algorithm implementation of this method is more complex and requires higher hardware processors.

The methods based on model observation use a disturbance observer to estimate error voltages [14–16], Furthermore, it not only reduces the sixth harmonic as in many other compensation methods but also deals with its multiples concurrently. In [15], this paper introduces a current harmonic elimination method based on a disturbance observer (DOB), Although the DOB was shown to be able to satisfactorily operate under a constant change in the rotational speed of the machine, this method has not been verified for the dynamic response performance during motor startup. In [17], the expression of the inverter input current was derived by considering the deadtime effect. However, these models are not suitable for closed-loop control systems such as VSI-fed field-oriented control (FOC) PMSM servo systems. The control scheme using two extended state observers (ESO) is proposed in [14], which provides a strong ability to suppress dead-time effects, but the effect of this method can be further improved. In the following, the method using ESO [14] is compared with the method proposed in this paper.

In recent years, the number of studies related to the application of fractional controllers has been increasing. Fractional order control achieves better performance than conventional integer-order control, which can provide an opportunity to adjust better the dynamical characteristics of the control system [18–21]. And fractional-order proportional integral (FOPI) control has been widely used for servo systems [20]. Therefore, the FOPI controller is applied in our proposed dead-time compensation method to pursue advanced robustness.

This paper proposes a dead-time compensation method for a PMSM servo system with an optimal FOPI error voltage control. The proposed method based on the model of PMSM can calculate the error between the reference and output voltages, and the FOPI controllers can make the error voltages of the d-axis and q-axis converge to zero quickly. The proposed control strategy uses the PSO algorithm to design the parameters of the FOPI controller, considering the nonlinearity of the dead-time effect. The proposed dead-time compensation strategy can reduce the current disturbance in the VSI system. A PMSM system is used to validate the proposed method. Simulation and experimental results are presented to demonstrate the effectiveness of the proposed method.

The main contributions of this paper are as follows. (1) This paper proposes a dead-time compensation method for PMSM servo systems with optimal FOPI error voltage control. The method proposed in this paper can not only eliminate low-frequency harmonic disturbances but also has a good suppression effect on high-frequency harmonics. A voltage model with dead-time effect and parameter error of permanent magnet synchronous motor is established. The actual error voltage is calculated based on the model and actual voltage of the permanent magnet synchronous motor. Considering the parameter error of the permanent magnet synchronous motor and the voltage error caused by the dead-time effect, the FOPI controller is used to calculate the compensation voltage. (2) An improved particle swarm optimization (PSO) algorithm is utilized to design the parameters of the FOPI controller, and in order to eliminate the dead-time effect, the optimal fitness function is designed. Compared with other optimization algorithms, the improved PSO algorithm can achieve a faster convergence speed in the error voltage controller parameter design. (3) Through theoretical and experimental analysis, it is proven that the method proposed in this paper can have good error voltage control performance and robustness in the case of motor parameter errors.

The rest of this article is organized as follows. The formula derivation process for the error voltage caused by the dead-time effect is presented in Section 2. In Section 3, a dead-time compensation method with optimal FOPI error voltage control is proposed, and the parameter tuning procedure of the FOPI controller is also presented. The simulation and experiments using the proposed dead-time compensation method are presented in Sections 4 and 5, compared with the dead-time compensation method using optimal integer-order proportional integral (IOPI) control, the dead-time compensation method using ESO [14] and the dead-time-related harmonic minimization method [4]. Finally, the conclusion is given in Section 6.

2. Analysis of Dead-Time Effect

The typical three-phase PWM inverter with PMSM load is illustrated in Figure 1.

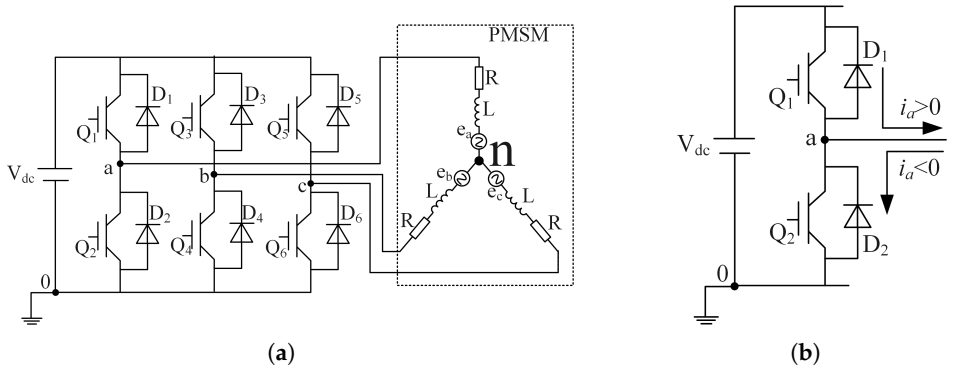

Figure 1. Model component. (**a**) Three-phase PWM drive system. (**b**) One phase leg of the PWM inverter.

In practice, a dead-time, T_d, is inserted in the gating signals to guarantee the safety of the VSI system. The gating signals with the dead time added are shown in Figure 2b. During the dead-time period T_d, the switches in Figure 1 are turned off, and the terminal voltage V_{a0} is determined by the direction of the a-phase current [22]. Figure 2c is the ideal terminal voltage. Considering the dead time and the turn ON/OFF delay, the terminal voltage is illustrated in Figure 2d,e. In this case, the a-phase average terminal voltage error ΔV_{a0} over one PWM period can be given as

$$\Delta V_{a0} = V_{err} * sign(i_a), \quad sign(i_a) = \begin{cases} -1, & i_a < 0 \\ 1, & i_a > 0 \end{cases} \tag{1}$$

where ΔV_{a0} is the a-phase average terminal voltage error over one PWM period, $sign(i_a)$ is the direction of the a-phase current, and V_{err} represents the magnitude of the terminal voltage error, which is defined as

$$V_{err} = \frac{T_d + T_{on} - T_{off}}{T_s} V_{dc} + V_{drop} \tag{2}$$

where V_{dc} is the dc-link voltage, T_d is the dead time, T_s is the PWM carrier period, T_{on} is the turn-on time delay of the switching device, T_{off} is the turn-off time delay of the switching device, and V_{drop} is the forward voltage drop of the switching device and of the diode.

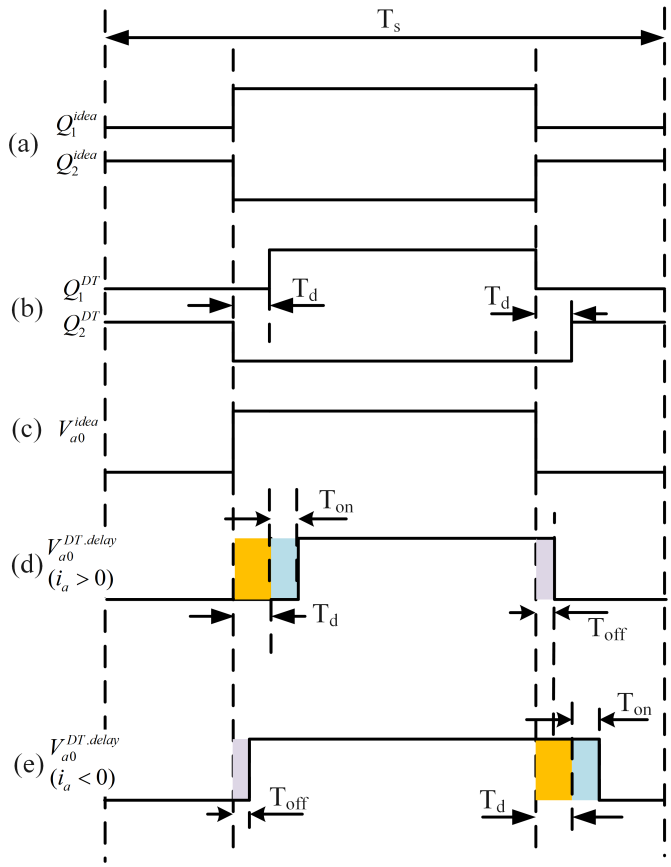

Figure 2. Switching pattern and terminal voltages: (**a**) Ideal gate signals. (**b**) Real gate signals with dead-time; (**c**) Ideal terminal voltage; (**d**) terminal voltage with dead-time and time delay when $i_a > 0$; (**e**) Actual terminal voltage with dead-time and time delay when $i_a < 0$.

In a similar way, the distorted voltage errors of other phases can be obtained. The error voltages in the three-phase stationary reference frame are obtained as

$$\begin{cases} \Delta u_{an} = \frac{1}{3}(2\Delta V_{a0} - \Delta V_{b0} - \Delta V_{c0}) \\ \Delta u_{bn} = \frac{1}{3}(2\Delta V_{b0} - \Delta V_{a0} - \Delta V_{c0}) \\ \Delta u_{cn} = \frac{1}{3}(2\Delta V_{c0} - \Delta V_{a0} - \Delta V_{b0}) \end{cases} \tag{3}$$

where ΔV_{a0}, ΔV_{b0}, and ΔV_{c0} are the three-phase terminal voltage errors of VSI and Δu_{an}, Δu_{bn}, and Δu_{cn} are the phase voltage errors of the PMSM in the three-phase stationary reference frame.

The error voltages in the stationary frame can be transformed to the synchronous reference frame as

$$\begin{bmatrix} \Delta u_{dt} \\ \Delta u_{qt} \end{bmatrix} = T_{2s/2r} \cdot T_{3s/2s} \cdot \begin{bmatrix} \Delta u_{an} \\ \Delta u_{bn} \\ \Delta u_{cn} \end{bmatrix} \tag{4}$$

$$T_{3s/2r} = \frac{2}{3}\begin{bmatrix} 1 & -1/2 & -1/2 \\ 0 & \sqrt{3}/2 & -\sqrt{3}/2 \end{bmatrix} \tag{5}$$

$$T_{2s/2r} = \begin{bmatrix} \cos(\theta_e) & \sin(\theta_e) \\ -\sin(\theta_e) & \cos(\theta_e) \end{bmatrix} \tag{6}$$

where Δu_d and Δu_q are the d-axis and q-axis error voltages of the PMSM in the synchronous reference frame caused by dead-time effect, $T_{2s/3r}$ is the Park's transformation, and $T_{2s/3r}$ is Clark's transformation, θ_e is the rotor electrical position.

The analysis mentioned above demonstrates that the dead-time error voltage can be influenced by current polarity, the turn ON/OFF delay, the voltage drop of the switching device, and the diode. It is inaccurate for detecting current polarity because of the clamping of current around the zero-crossing point. Due to the change in operating conditions, such as temperature, many parameters affecting dead-time compensation are difficult to measure. Thus, it takes work to compensate for the effect of dead time directly.

3. Proposed Dead-Time Compensation Strategy

3.1. Error Voltage Calculation Based on PMSM Model

The dynamic model of PMSM in the synchronous reference frame can be represented as (7).

$$\begin{bmatrix} u_d \\ u_q \end{bmatrix} = \begin{bmatrix} R_s + L_s p & -w_e L_q \\ w_e L_s & R_s + L_q p \end{bmatrix} \begin{bmatrix} i_d \\ i_q \end{bmatrix} + \begin{bmatrix} 0 \\ w_e \psi_f \end{bmatrix} \tag{7}$$

where u_d is the d-axis actual voltage, u_q is the q-axis actual voltage, i_d is the d-axis current, i_q is the q-axis current, and L_s, R_s, ω_e, and ψ_f represent the stator inductance, resistance, rotor electrical angular velocity, and rotor flux linkage.

Therefore, the dynamic model of PMSM in the discrete-time domain is represented as:

$$\begin{bmatrix} u_d(k-1) \\ u_q(k-1) \end{bmatrix} = \begin{bmatrix} R_s + \frac{L_s}{T_s} & -w_e L_s \\ w_e L_s & R_s + \frac{L_s}{T_s} \end{bmatrix} \begin{bmatrix} i_d(k) \\ i_q(k) \end{bmatrix} - \frac{L_s}{T_s} \begin{bmatrix} i_d(k-1) \\ i_q(k-1) \end{bmatrix} + \begin{bmatrix} 0 \\ w_e \psi_f \end{bmatrix} \tag{8}$$

where k represents the kth PWM period, $i_d(k)$ and $i_q(k)$ are the d-axis current and q-axis current of the kth PWM period, $u_d(k-1)$ and $u_q(k-1)$ are the d-axis voltage and q-axis voltages of the $k-1$ PWM period, and T_s is the sampling period.

Since proper motor parameters cannot be obtained in practice, the equivalent error voltage caused by the motor parameter error can be obtained through (9)

$$\begin{bmatrix} err_d(k-1) \\ err_q(k-1) \end{bmatrix} = \begin{bmatrix} R_s + \frac{L_s}{T_s} & -w_e L_s \\ w_e L_s & R_s + \frac{L_s}{T_s} \end{bmatrix} \begin{bmatrix} i_d(k) \\ i_q(k) \end{bmatrix} - \frac{L_s}{T_s} \begin{bmatrix} i_d(k-1) \\ i_q(k-1) \end{bmatrix} - \begin{bmatrix} R_c + \frac{L_c}{T_s} & -w_e L_c \\ w_e L_s & R_c + \frac{L_c}{T_s} \end{bmatrix} \begin{bmatrix} i_d(k) \\ i_q(k) \end{bmatrix} + \frac{L_c}{T_s} \begin{bmatrix} i_d(k-1) \\ i_q(k-1) \end{bmatrix} \tag{9}$$

where L_c and R_s represent the nominal stator inductance, nominal resistance, and err_d and err_q represent the equivalent error voltage caused by the motor parameter error.

Affected by the dead-time effect of the inverter, there is an error between the reference voltage and the output voltage. According to (8), the dynamic model of PMSM, including the error voltage in the discrete-time domain, can be represented as:

$$\begin{bmatrix} {u_d}^*(k-1) \\ {u_q}^*(k-1) \end{bmatrix} = \begin{bmatrix} R_c + \frac{L_c}{T_s} & -w_e L_c \\ w_e L_s & R_c + \frac{L_c}{T_s} \end{bmatrix} \begin{bmatrix} i_d(k) \\ i_q(k) \end{bmatrix} - \frac{L_c}{T_s} \begin{bmatrix} i_d(k-1) \\ i_q(k-1) \end{bmatrix} + \begin{bmatrix} err_d(k-1) \\ err_q(k-1) \end{bmatrix} + \begin{bmatrix} \Delta u_{dt}(k-1) \\ \Delta u_{qt}(k-1) \end{bmatrix} \tag{10}$$

where ${u_d}^*$ and ${u_q}^*$ represent the d-axis and q-axis reference voltage of the $k-1$ PWM period and $\Delta u_{dt}(k-1)$ and $\Delta u_{qt}(k-1)$ represent d-axis and q-axis error voltages caused by dead-time effect.

Based on (10), the total error voltage caused by the dead-time effect and motor parameter error in the synchronous reference frame can be calculated using (12).

$$\begin{cases} \Delta u_q(k-1) = \Delta u_{dt}(k-1) + err_d(k-1) \\ \Delta u_d(k-1) = \Delta u_{qt}(k-1) + err_q(k-1) \end{cases} \tag{11}$$

$$\begin{cases} \Delta u_q(k-1) = {u_{qc}}^*(k-1) - u_q(k-1) \\ \Delta u_d(k-1) = {u_d}^*(k-1) - u_{dc}(k-1) \end{cases} \tag{12}$$

where u_{dc} and u_q represent the actual nominal voltages of the d-axis and q-axis calculated from the nominal motor parameters, $\Delta u_d(k-1)$ and $\Delta u_q(k-1)$ represent d-axis and q-axis error voltages.

Therefore, to control the error voltage caused by the dead-time effect and the uncertainty error voltage caused by motor parameter error, it is necessary to use a FOPI controller with high control performance.

3.2. Compensation Method with Optimal FOPI Error Voltage Control

Figure 3 shows the system control block diagram. The actual voltage calculation module is shown in Figure 4, which can be represented by (12). When using the compensation method with optimal FOPI error voltage control, the system control block diagram is also shown in Figure 3. The compensation method with optimal FOPI error voltage control uses the FOPI controller as the error voltage controller. The control objective is to make the actual d-axis and q-axis voltages of the motor follow the reference voltages. The error voltage caused by the dead-time effect can be reduced as much as possible.

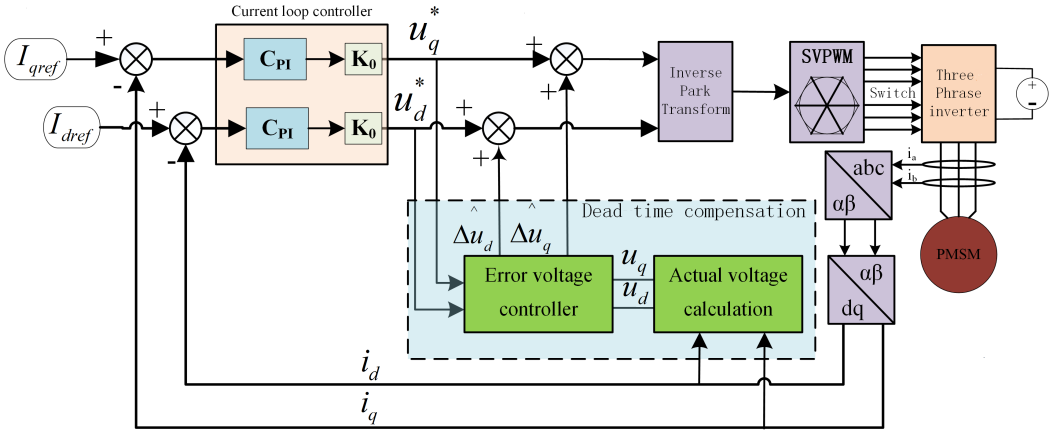

Figure 3. Block diagram of the system control.

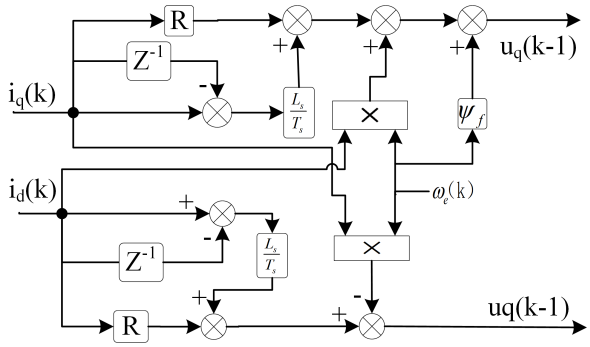

Figure 4. The actual voltage calculation module.

G_{FOPI} is the transfer function of the FOPI controller, which is shown as (13).

$$G_{FOPI} = k_p + k_i/s^{\alpha} \tag{13}$$

where k_p and k_i are proportional and integral gains and α is a fractional order. In this paper, we consider $\alpha \in (0, 2)$.

According to the impulse response invariance method [23], the higher the order, the higher the accuracy. However, a high approximation order results in more operating time for the microprocessor. Therefore, in practical applications, the approximation order is chosen based on control performance requirements and hardware constraints. The z-domain expression of the fractional operator $1/s^{\alpha}$ can be obtained with

$$\frac{1}{s^{\alpha}} = \frac{\text{NUM}}{\text{DEN}} \tag{14}$$

$$\text{NUM} = n_0 + n_1 z^{-1} + n_2 z^{-2} + \ldots + n_5 z^{-5} \tag{15}$$

$$\text{DEN} = 1 + d_1 z^{-1} + d_2 z^{-2} + \ldots + d_5 z^{-5} \tag{16}$$

where n_i and d_i(i = 1…5) are the discretization coefficients of fractional-order operators.

When using the compensation method with optimal FOPI error voltage control, the error voltage controller is shown in Figure 5 and $\Delta\hat{u}_q(k)$ is the q-axis compensation voltage. The calculation is as in (17).

$$\Delta\hat{u}_q(k) = P_q(k) + I_q^{fo}(k) \tag{17}$$

where $P_{\mathrm{q}}(k)$ and $I_{\mathrm{q}}^{fo}(k)$ represent the proportional and fractional-order integral terms of the q-axis FOPI error voltage controller of the kth PWM period, as in (18) and (19).

$$P_{\mathrm{q}}(k) = kp_q * \Delta u_q(k-1) \tag{18}$$

$$\begin{aligned} I_{\mathrm{q}}^{fo}(k) =& ki_q * \big(n_0\Delta u_q(k-1) + n_1\Delta u_q(k-2) + n_2\Delta u_q(k-3) + n_3\Delta u_q(k-4) + \\ & n_4\Delta u_q(k-5) + n_5\Delta u_q(k-6) - d_1 I_{\mathrm{q}}^{fo}(k-1) - d_2 I_{\mathrm{q}}^{fo}(k-2) - \\ & d_3 I_{\mathrm{q}}^{fo}(k-3) - d_4 I_{\mathrm{q}}^{fo}(k-4) - d_5 I_{\mathrm{q}}^{fo}(k-5)\big) \end{aligned} \tag{19}$$

The $\Delta\hat{u}_d(k)$ is the d-axis compensation voltage. The calculation is as in (20).

$$\Delta\hat{u}_d(k) = P_d(k) + I_d^{fo}(k) \tag{20}$$

where $P_{\mathrm{d}}(k)$ and $I_{\mathrm{d}}^{fo}(k)$ represent the proportional and fractional-order integral terms of the d-axis FOPI error voltage controller of the kth PWM period, as in (21) and (22).

$$P_d(k) = kp_d * \Delta u_d(k-1) \tag{21}$$

$$\begin{aligned} I_d^{fo}(k) =& ki_d * (n_0\Delta u_d(k-1) + n_1\Delta u_d(k-2) + n_2\Delta u_d(k-3) + n_3\Delta u_d(k-4) + \\ & n_4\Delta u_d(k-5) + n_5\Delta u_d(k-6) - d_1 I_d^{fo}(k-1) - d_2 I_d^{fo}(k-2) \\ & - d_3 I_d^{fo}(k-3) - d_4 I_d^{fo}(k-4) - d_5 I_d^{fo}(k-5)) \end{aligned} \tag{22}$$

where $\Delta\hat{u}_q(k)$ and $\Delta\hat{u}_d(k)$ are the q-axis and d-axis compensation voltages of the kth PWM period, kp_d and ki_d are proportional and integral gains of d-axis FOPI error voltage controller, and kp_q and ki_q are proportional and integral gains of q-axis FOPI error voltage controller.

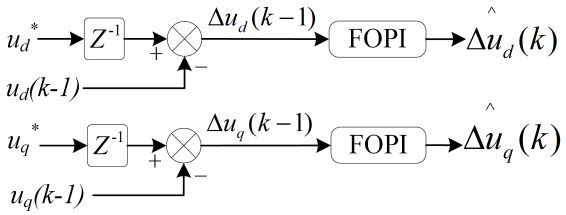

Figure 5. FOPI error voltage controller.

3.3. Compensation Method with Optimal IOPI Error Voltage Control

The FOPI controller can be superior to the IOPI in control performance and robustness. To prove the necessity and superiority of using the FOPI controller, the IOPI controller is used for error voltage control and compared with the FOPI controller. The compensation method with optimal integer order proportional integral (IOPI) error voltage control uses the IOPI controller as the error voltage controller.

$\mathrm{G_{IOPI}}$ is the transfer function of the IOPI controller, which is shown as in (23).

$$\mathrm{G_{IOPI}} = k_p + k_i/s \tag{23}$$

where k_p and k_i are proportional and integral gains.

When using the compensation method with optimal IOPI error voltage control, the error voltage controller is shown in Figure 6. The compensation voltages are the output of the IOPI controllers. The calculation is as in (24) and (25).

$$\Delta\hat{u}_q(k) = k_{pq} * \Delta u_q(k-1) + k_{iq} * T_s \sum_{i=1}^{k-1} \Delta u_q(i) \tag{24}$$

$$\Delta\hat{u}_d(k) = k_{pd} * \Delta u_d(k-1) + k_{id} * T_s \sum_{i=1}^{k-1} \Delta u_d(i) \tag{25}$$

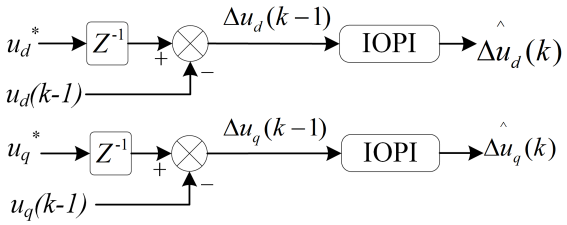

Figure 6. IOPI error voltage controller.

In the above equations (24) and (25), $\Delta\hat{u}_q(k)$ and $\Delta\hat{u}_d(k)$ are the q-axis and d-axis compensation voltages of the kth PWM period, k_{pd} and k_{id} are proportional and integral gains of d-axis IOPI error voltage controller, and k_{pq} and k_{iq} are proportional and integral gains of q-axis IOPI error voltage controller.

3.4. Parameter Design of Error Voltage Controller Based on Improved PSO Algorithm

Due to its simplicity and ease of implementation with only a few parameters, the particle swarm optimization (PSO) algorithm has shown desired optimization performance in continuous optimization problems, and discrete optimization problems [24–26]. Because of the non-linear characteristics of the dead-time effect, it is challenging to use frequency domain analysis to design the parameters of the error voltage controller. In this paper, the improved PSO algorithm is presented to develop the parameters of the error voltage controller, and the process is shown in Figure 7.

In Figure 7, the position of the particle represents the parameters of the error voltage controller, and the fitness function represents the performance index of the compensation effect. When using the method with optimal IOPI error voltage control, the position of the particles corresponds to the parameters of the IOPI controllers. When using the method with optimal FOPI error voltage control, the position of the particles corresponds to the parameters of the FOPI controllers.

The following is the optimization procedure. First, a particle swarm is generated, and the positions of the particles are sequentially assigned to the parameters of the error voltage controller (IOPI controller or FOPI controller). Then the performance index corresponding to the set of parameters can be obtained by the simulation model of the control system. By evaluating the fitness function, the optimal fitness value and particle position can be obtained. Finally, it is judged whether the maximum number of iterations is reached. If not, the operation of updating the particle is performed. If the number of iterations equals the maximum number of iterations, the algorithm obtains the optimal position.

The update operation of particles mainly includes speed update and position update, which are calculated according to (26).

$$\begin{cases} v_{i+1} = \omega_i v_i + c_1 r_1 (P_i - x_i) + c_2 r_2 (G_i - x_i) \\ x_{i+1} = x_i + v_{i+1} \end{cases} \tag{26}$$

where x_i is the particle's position of the ith iteration, i is the number of iteration, v_i is the particle's velocity of the ith iteration, x_{i+1} and v_{i+1} are the position and velocity of the the $i+1$ iteration, and ω_i is the inertia weight at the ith iteration. c_1 and c_2 are the acceleration coefficients, c_1 and c_2 control the relative proportion of cognition and social interaction in the swarm. r_1 and r_2 are random numbers between [0,1], P_i is the optimal position of

a single particle until the ith iteration, and G_i is the optimal position of the entire particle swarm until the ith iteration.

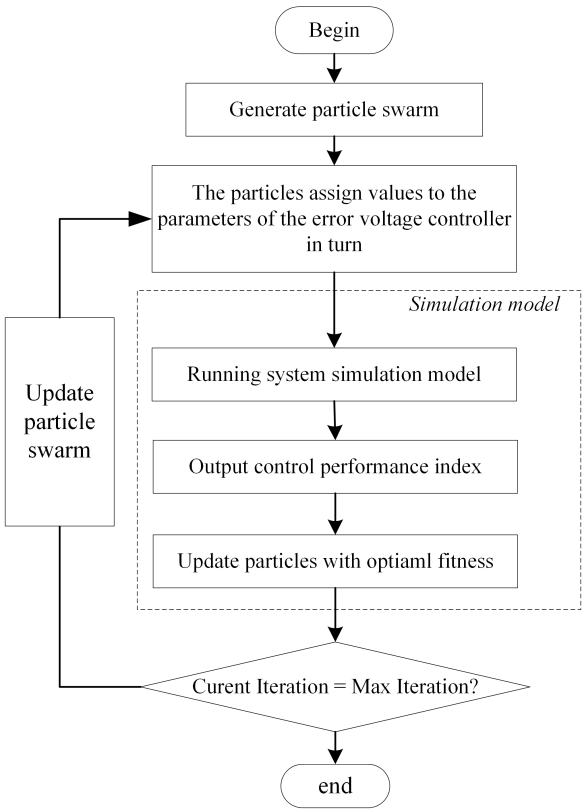

Figure 7. The process of parameter design of error voltage controller.

To dynamically adjust the inertia weight, we consider $\omega_i \in [\omega_{min}, \omega_{max}]$, and the inertia weight at the ith iteration is as in (27).

$$\omega_i = \omega_{\max} - \frac{\omega_{\max} - \omega_{\min}}{\text{Iter}_{\max}} \cdot i \tag{27}$$

where ω_{min} and ω_{max} are constants, the $iter_{max}$ is maximum number of iteration.

As in (28), the acceleration coefficient c_1 keeps decreasing over time, and the acceleration coefficient c_2 keeps increasing over time.

$$\begin{cases} c_1 = (c_{1f} - c_{1i}) \frac{i}{\text{Iter}_{\max}} + c_{1i} \\ c_2 = (c_{2f} - c_{2i}) \frac{i}{\text{Iter}_{\max}} + c_{2i} \end{cases} \tag{28}$$

where c_{1i}, c_{1f}, c_{2i}, and c_{2f} are constants, which are the initial and final values of c_1 and c_2, and the $\text{Iter}_{\max}$ is the maximum number of iteration.

The purpose of the error voltage controller is to minimize the q-axis voltage error and the d-axis voltage error. The q-axis current ripple directly causes the torque ripple. It greatly influences the system's control performance, so this paper pays more attention to the voltage error control effect of the q-axis. Referring to the evaluation index of ITAE, the fitness function is set to J_{ITAE}, as in (29).

$$J_{ITAE} = 4 * \int_0^\infty t|\Delta u_q|dt + \int_0^\infty t|\Delta u_d|dt \tag{29}$$

where $\Delta u_d(k)$ and $\Delta u_q(k)$ represent the d-axis and q-axis error voltages of the kth PWM period. t is the running time of the system.

When using the compensation method with optimal IOPI error voltage control, the particle position x_i is shown in (30).

$$x_i = \begin{bmatrix} k_{pd} & k_{id} & k_{pq} & k_{iq} \end{bmatrix} \tag{30}$$

where k_{pd} and k_{id} are proportional and integral gains of the d-axis IOPI error voltage controller and k_{pq} and k_{iq} are proportional and integral gains of q-axis IOPI error voltage controller.

For designing the parameters of the IOPI controller, the configuration of the improved PSO algorithms is shown in Table 1.

Based on the configuration in Table 1, the parameters of the IOPI controller are optimized by the PSO algorithm. The convergence curve of the optimal fitness function value with the number of iterations is shown in Figure 8.

Table 1. The configuration of the improved PSO algorithm.

For Optimal IOPI Controler		For Optimal FOPI Controller	
populations	40	populations	40
$\text{Iter}_{\max}$	40	$\text{Iter}_{\max}$	40
$\omega_{\max}$	0.8	$\omega_{\max}$	0.8
$\omega_{\min}$	0.2	$\omega_{\min}$	0.2
c_{1f}	0.3	c_{1f}	0.3
c_{1i}	2.5	c_{1i}	2.5
c_{2i}	0.3	c_{2i}	0.3
c_{2f}	2.5	c_{2f}	2.5
$v_{\max}$	[3,40,3,40]	$v_{\max}$	[3,40,3,40,0.2,0.2]
$v_{\min}$	[−3,−40,−3,−40]	$v_{\min}$	[−3,−40,−3,−40,−0.2,−0.2]
$x_{\max}$	[2,1000,20,1000]	$x_{\max}$	[2,1000,20,1000,0,0]
$x_{\min}$	[0,0,0,0]	$x_{\min}$	[0,0,0,0,−2,−2]

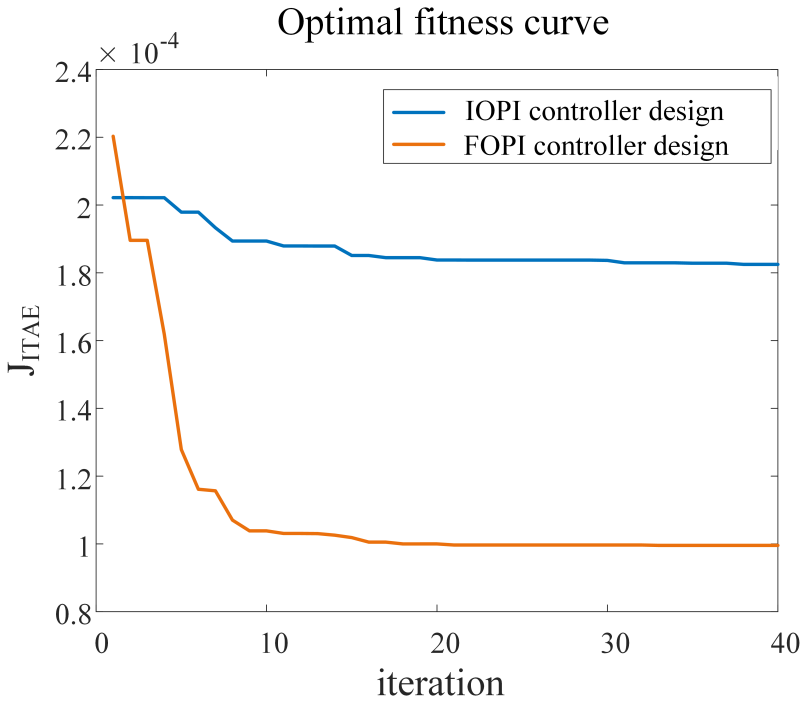

Figure 8. PSO algorithm Optimal fitness function value in FOPI/IOPI controller design.

The parameter iteration result of the IOPI controller based on the improved PSO algorithm is shown in Table 2.

When using the compensation method with optimal FOPI error voltage control, the particle position x_i is shown in (31)

$$x_i = \left[kp_d, ki_d, kp_q, ki_q, \alpha_d, \alpha_q\right] \tag{31}$$

where kp_d and ki_d are proportional and integral gains of the d-axis FOPI error voltage controller, kp_q and ki_q are proportional and integral gains of q-axis FOPI error voltage controller, α_d is the fractional order of the d-axis FOPI error voltage controller, and α_q is fractional order of q-axis FOPI error voltage controller.

For designing the parameters of the FOPI controller, the configuration of the improved PSO algorithms is shown in Table 1.

Based on the configuration in Table 1, the parameters of the FOPI controller are optimized using the PSO algorithm. The convergence curve of the optimal fitness function value with the number of iterations is shown in Figure 8.

Table 2. The parameter iteration result.

Paramters of IOPI Controller		Paramters of FOPI Controller	
k_{pd}	3.05745	kp_d	2.186
k_{id}	431.402	ki_d	491.66
k_{pq}	2.7419	kp_q	1.693
k_{iq}	707.891	ki_q	503.683
		α_d	0.651
		α_q	0.722

The parameter iteration result of the FOPI controller is shown in Table 2.

The Artificial Bee Colony (ABC) Algorithm is an optimization algorithm based on intelligent behavior.

For the parameter design of the IOPI/FOPI controller, the parameter optimization curve of the ABC algorithm is shown in Figure 9 [27]. The comparison of the iterative optimization results of the ABC algorithm and the PSO algorithm is shown in Table 3, it can be seen that the optimal fitness values obtained by the two algorithms are approximately equal, which proves that the controller parameters obtained in Table 2 are the global optimal solution. Compared with the ABC algorithms, the improved PSO algorithm can achieve a faster convergence speed in the error voltage controller parameter design.

Table 3. Comparison of optimal fitness function Values between ABC algorithm and PSO algorithm.

	IOPI Controller	FOPI Controller
Optimal fitness function value of PSO algorithm	1.8350×10^{-4}	9.9584×10^{-5}
Optimal fitness function value of ABC algorithm	1.8310×10^{-4}	9.9618×10^{-5}

The α_d is the fractional order of the d-axis FOPI error voltage controller. According to Table 2, α_d = 0.651. The discrete implementation of $1/s^{\alpha_d}$ can be obtained using the impulse response invariance method [23], and the comparison of discretization approximate bode graph and ideal bode graph is shown in Figure 10. The α_q is the fractional order of the q-axis FOPI error voltage controller, and the comparison of discretization approximate bode graph and ideal bode graph of $1/s^{\alpha_q}$ is shown in Figure 11.

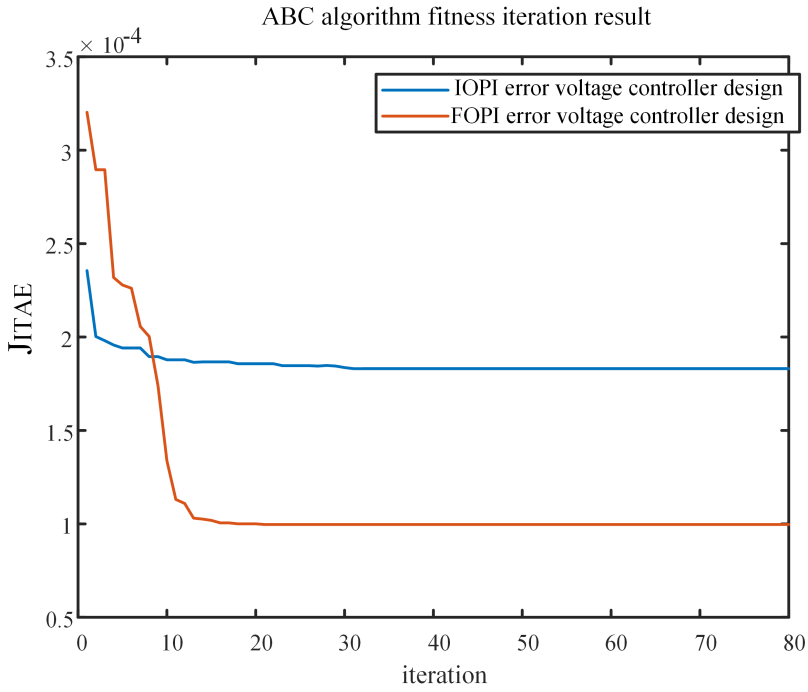

Figure 9. ABC algorithm Optimal fitness function value in FOPI/IOPI controller design.

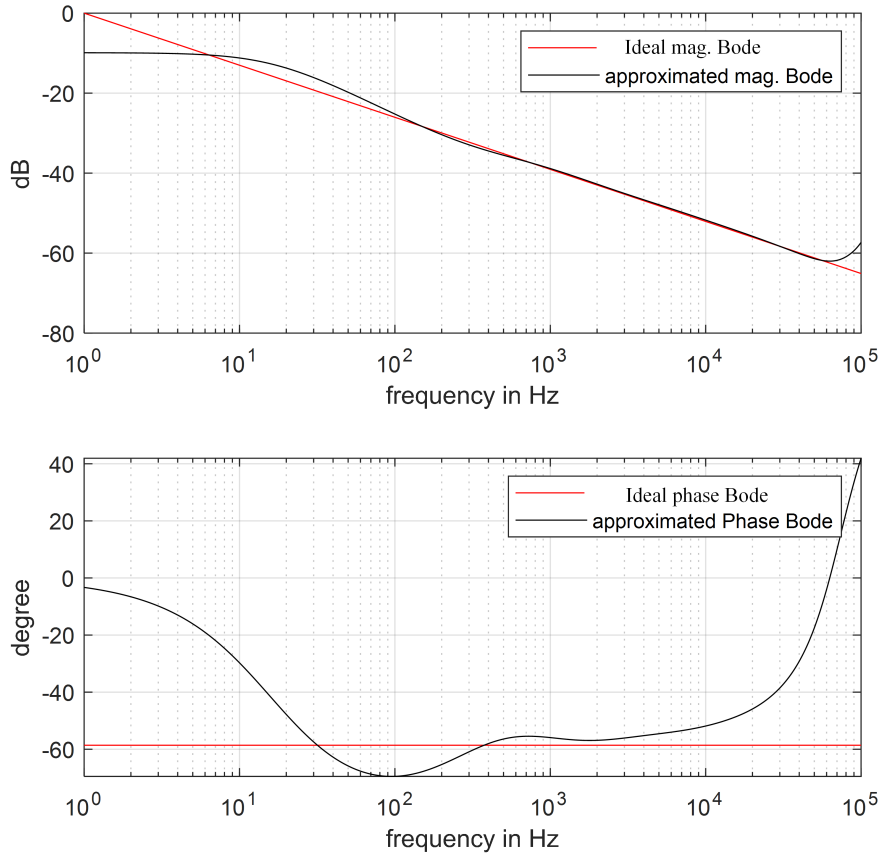

Figure 10. The comparison of discretization approximate bode graph and ideal bode graph of $1/s^{\alpha_d}$.

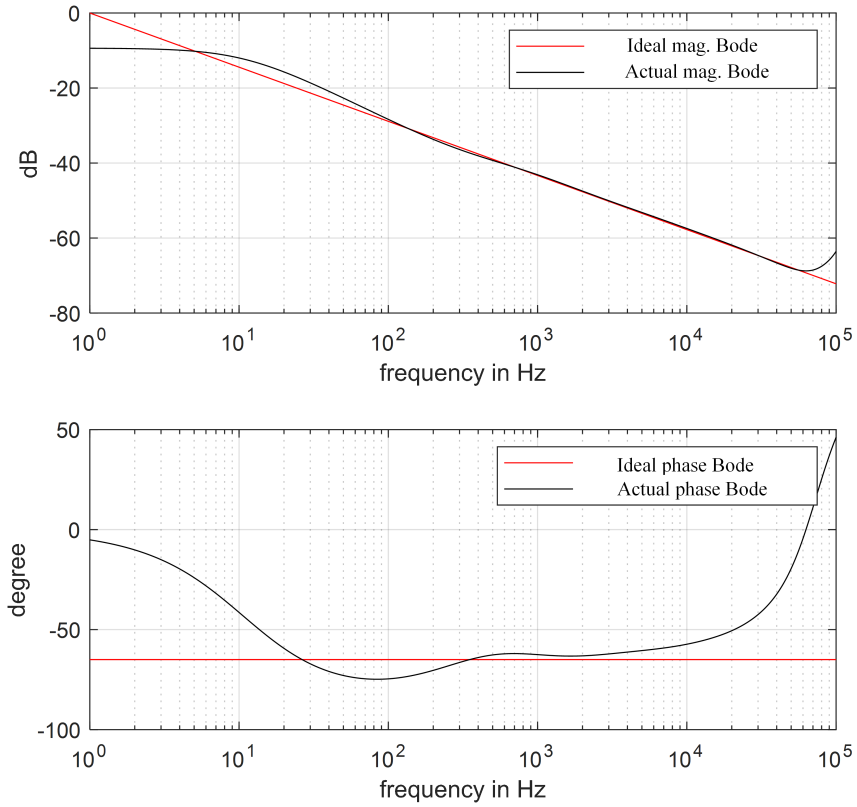

Figure 11. The comparison of discretization approximate bode graph and ideal bode graph of $1/s^{\alpha_q}$.

3.5. Parameters Design of Current Loop Controller and Speed Loop Controller

The PMSM current can be controlled with two PI controllers. Without dead-time compensation, the simplified PMSM current control system is shown in Figure 12.

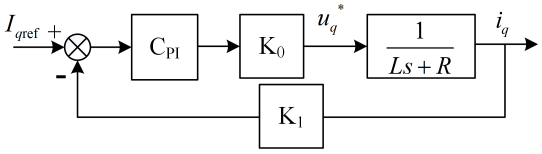

Figure 12. The simplified PMSM current control system.

The current loop controller model C_{PI} is as in (32)

$$C_{PI}(s) = K_{pc} + \frac{K_{ic}}{s} \tag{32}$$

where K_{pc} and K_{ic} are proportional and integral coefficients. The open-loop transfer function of the current loop is as follows:

$$\begin{aligned} G_{co}(s) &= K_0 K_1 C_{PI}(s) \frac{1}{L_s s + R_s} \\ &= K_0 K_1 \left(\frac{K_{pc} s + K_{ic}}{s} \right) \frac{1}{L_s s + R_s}. \end{aligned} \tag{33}$$

where K_0 and K_1 are constants. K_0 represents the voltage conversion coefficient, and K_1 represents the current conversion coefficient. L_s and R_s represent the stator inductance and resistance.

According to the existing system, K_0 = 179.561 and K_1 = 1/19.2. The current controller is designed by the cancellation method with relationship K_{pc}/K_{ic} = L/R [28]. The gain crossover frequency is set as ω_c = 2000 rad/s,

$$|G_{co}(j\omega_c)| = 1 \tag{34}$$

According to (34), we can get the parameters of current loop controller as follows:

$$K_{pc} = \frac{\omega_c L_s}{K_0 K_1}, \tag{35}$$

$$K_{ic} = \frac{K_{pc} R_s}{L_s} = \frac{\omega_c R_s}{K_0 K_1}. \tag{36}$$

4. Simulation Results

The proposed method is compared with the method without compensation to demonstrate the effectiveness of the dead-time compensation method with optimal FOPI error voltage control. The proposed method is compared with the method using optimal IOPI error voltage control and the compensation with extended state observers (ESO) [14] to indicate higher performance using optimal FOPI control. In order to prove that the FOPI error voltage control method has a good ability to eliminate current harmonics, this dead-time-related harmonic minimization method [4] is compared with the proposed method. The simulation model is built using MATLAB/Simulink, which has the same control scheme and parameters as the drive system. The dead time in the gate of power switches is 2.1 µs. The simulation control block diagram is shown in Figure 3, the Iq_{ref} is set to 1 A, and the Id_{ref} is set to 0 A. According to (35) and (36), The parameters of the current loop controller can be calculated as K_{pc} = 1.4018 and K_{ic} = 121.8973. The parameters of the error voltage controller are shown in Table 2. Other specifications of the simulation drive system are given in Table 4.

Table 4. Specification of experimental drive system.

Parameters of PMSM		Specification of PWM Inverter	
Pole pairs	5	DC link	310 [V]
Resistance (Rs)	0.38 [Ω]	PWM period	50 [µs]
Inductance (Ls)	4.37 [mH]	Turn-on/off delay	180/320 [µs]
Flux linkage (lam)	0.066 [Wb]	Dead-time	2.1 [µs]
Inertia (J)	0.027 [kg·m^2]	IGBT/Diode Ron	36 [mΩ]
viscous daping (B)	0.0502 [N·m·s]	Saturation Volt	1.1 [V]

4.1. Current Closed-Loop Simulation

The simulation result of I_q current is shown in Figure 13 and Table 5. As we can see, the I_q current of the method without compensation is much distorted because of the dead-time effect, and the torque ripple in the steady state is very severe. When using the dead-time compensation method with optimal FOPI error voltage control, the current ripple can be significantly eliminated, and the tracking performance can be improved. Compared with the IOPI error voltage control and the compensation with ESO [14], it can be seen that the method with optimal FOPI error voltage control can further improve tracking performance and reduce the current ripple of the I_q current. Compared with the compensation with ESO [14], the optimal FOPI error voltage control can effectively suppress high-frequency harmonic disturbance.

In the simulation, the comparison of the I_d current response under the three control strategies is shown in Figure 14 and Table 6. The dead-time compensation method with optimal FOPI error voltage control can significantly reduce the current disturbance caused by the dead-time effect, and the method with optimal FOPI error voltage control has a

more vital ability to suppress the disturbance of the I_d current than that using optimal IOPI error voltage control and the compensation method with ESO [14]. Figure 15 and Table 7 show the three-phase current response comparison results. The dead-time compensation method with optimal FOPI error voltage control can significantly eliminate the current distortion and reduce the current clamping around the zero-crossing point. The method's performance with optimal FOPI error voltage control is better than that of IOPI error voltage control, which proves that the proposed method has a better dead-time compensation effect. Compared with the compensation with ESO [14], the optimal FOPI error voltage control can effectively suppress high-frequency harmonic disturbance.

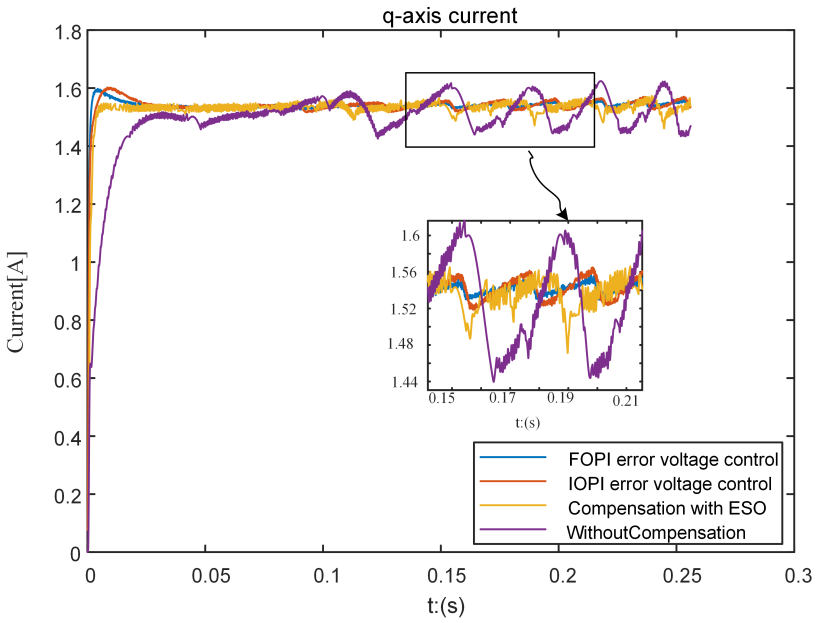

Figure 13. The comparison of I_q step current response of three control strategies.

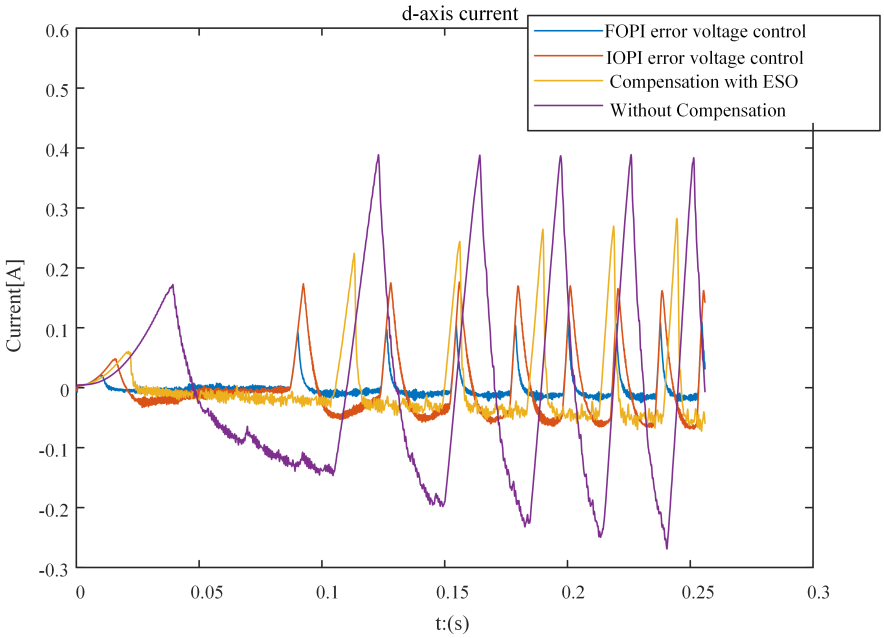

Figure 14. Comparison of I_d current response of three control strategies.

The q-axis error voltage simulation results are shown in Figure 16. The q-axis error voltage varies nonlinearly with increasing speed when using the method without compensation. The dead-time compensation method with optimal FOPI error voltage control can quickly make the error voltage converge to 0. The convergence speed of the proposed method is faster than that of the method using optimal IOPI error voltage control. The method with optimal FOPI error voltage control makes the q-axis error voltage converge to 0 faster than the method with optimal IOPI error voltage control.

Table 5. The performance index comparison of I_q step current response in the simulation.

	without Compensation	**IOPI**	**FOPI**	**ESO [14]**
overshoot (%)	9.05	4.53	4.767	0.0
rise time (s)	0.01825	0.0037	0.0017	0.00986
settling time (s)	\	0.03	0.024	0.00986
current ripple amplitude (A)	0.184	0.0359	0.0175	0.08467

Table 6. The performance index comparison of I_d step current response.

	without Compensation	**IOPI**	**FOPI**	**ESO [14]**
Current ripple amplitude (A)	0.671	0.23	0.097	0.33

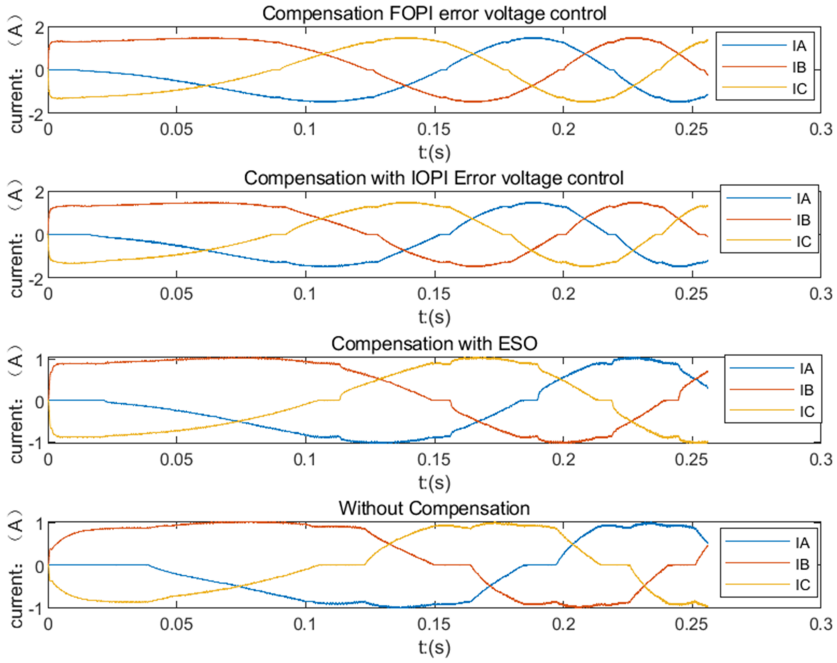

Figure 15. Comparison of three-phase current response of three control strategies.

Table 7. The performance index comparison of three-phrase current step current response.

	without Compensation	***IOPI***	**FOPI**	**ESO [14]**
Current clamping time (s)	0.0102	0.003258	0.001751	0.00482

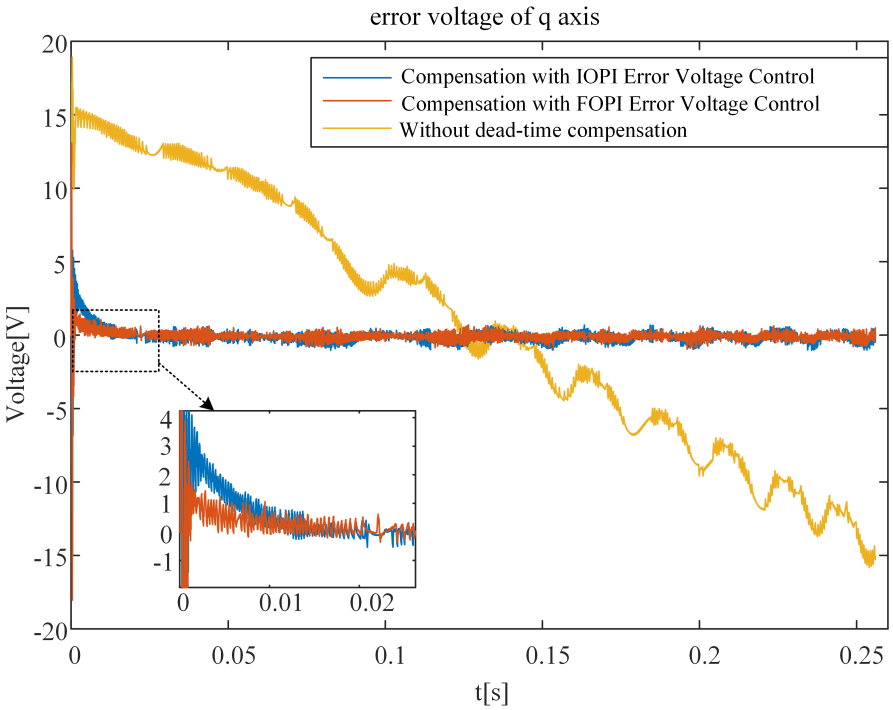

Figure 16. Comparison of the error voltage of q-axis.

The d-axis voltage error simulation results are shown in Figure 17. It can be seen that the d-axis error voltage fluctuates significantly under the influence of the dead-time effect, and the dead-time compensation method with optimal FOPI error voltage control can substantially reduce the d-axis error voltage.

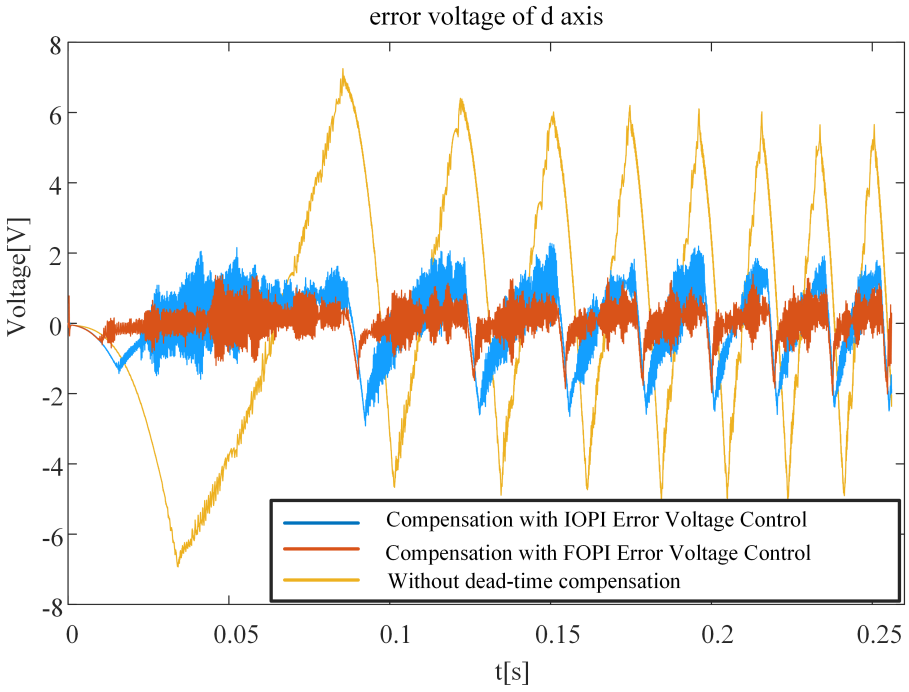

Figure 17. Comparison of the error voltage of d-axis in the simulation.

4.2. Speed Closed-Loop Simulation

In the case of keeping the motor speed constant at 200 r/min, compare the method proposed in this paper with the typical current harmonic elimination method. Observe and compare the three-phase current and its frequency spectrum. In [4], a dead-time-related harmonic minimization method based on proportional-integral (PI) controller tuning is proposed under the premise of keeping the same control strategy. In order to prove that the FOPI error voltage control method has a good ability to eliminate current harmonics, this dead-time-related harmonic minimization method [4] is compared with the proposed method.

The three-phase current simulation results and their spectral analysis for the dead-time-related harmonic minimization method and the method [4] proposed in this paper are shown in Figures 18 and 19. It can be seen from Figure 18 that the proposed method can more effectively eliminate the current clamping phenomenon caused by the dead-time effect. At the point where the current passes through 0, the current clamping time of the proposed method is shorter than the dead-time-related harmonic minimization method [4]. It can be seen from Figure 19 that the proposed method is better than the dead-time-related harmonic minimization method [4] in eliminating the dead-time effect harmonics.

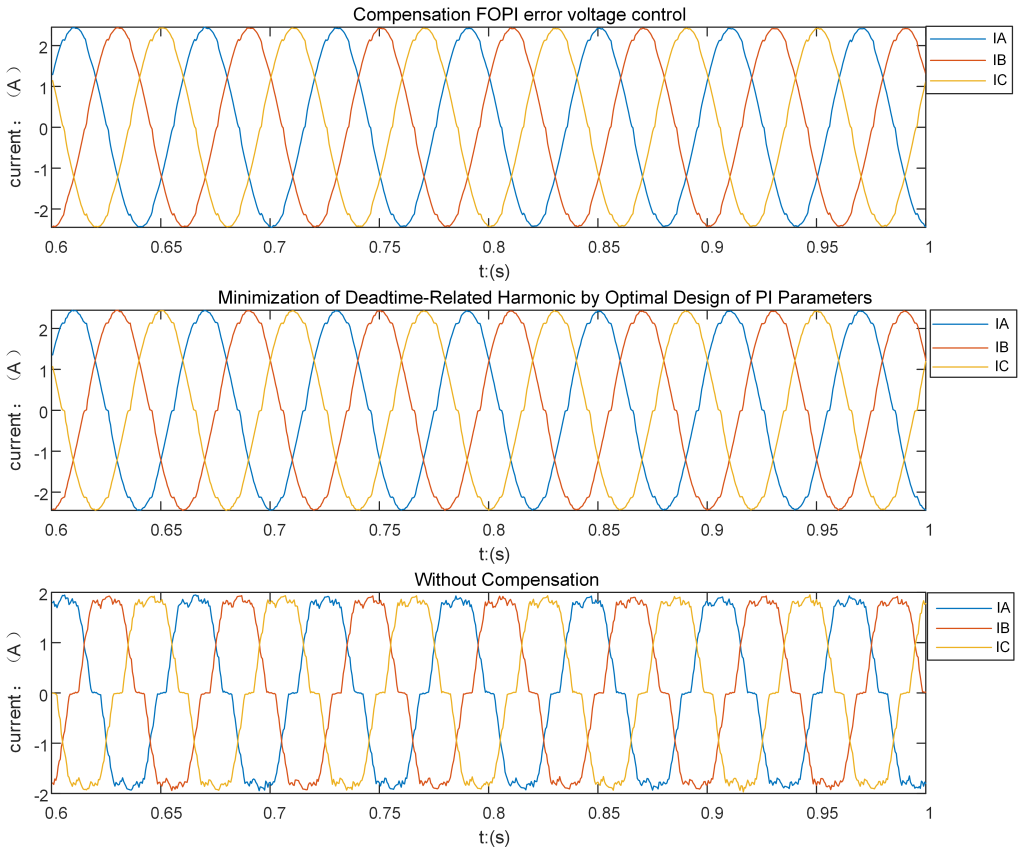

Figure 18. Comparison of three phase current response under 200 r/min speed conditions.

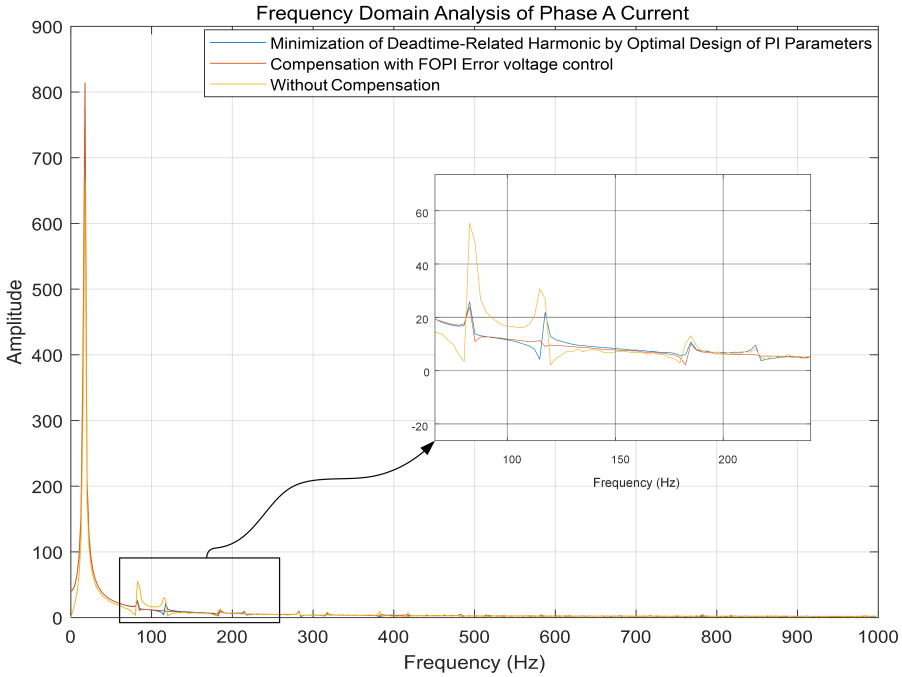

Figure 19. Frequency domain simulation analysis of A phase current under 200 r/min speed conditions.

4.3. Robustness Comparison for Motor Parameter Error

Due to the influence of motor characteristics, motor inductance and other parameters are easy to change during the experiment, so the verification of motor parameter uncertainty is added to the simulation. Three groups of motor parameters are randomly given within a certain range for simulation, and the effectiveness and robustness of the compensation method are verified by comparing the optimal FOPI error voltage control method and the optimal IOPI error voltage control method. The error and nominal motor parameters used in the simulation are shown in Table 8.

Table 8. Three groups of error motor parameters and motor actual parameters.

	Resistance (Ω)	**Inductance (mH)**	**Inertia ($kg \cdot m^2$)**	**Viscous Damping ($N \cdot m \cdot s$)**
error parameters (1)	0.514	4.90	0.0396	0.023
error parameters (2)	0.769	2.75	0.033	0.0299
error parameters (3)	0.769	1.96	0.0134	0.0172
actual parameters	0.38	4.37	0.027	0.05027

From Figures 20 and 21, it can be seen that the FOPI error voltage control method still has a good control effect when the motor parameter error occurs. The FOPI error voltage control method can effectively suppress the high-frequency harmonic disturbance caused by the motor parameter error. The control effect of the IOPI controller is poor, and the high-frequency harmonic disturbance cannot be effectively suppressed.

It can be seen from Figures 22 and 23 that in the case of errors in motor parameters, FOPI error voltage control still has good performance in eliminating the current clamping phenomenon and suppressing high-frequency harmonic disturbances. The control effect of FOPI error voltage control is better than that of IOPI error voltage control when there are errors in motor parameters, which proves the necessity of using the FOPI controller.

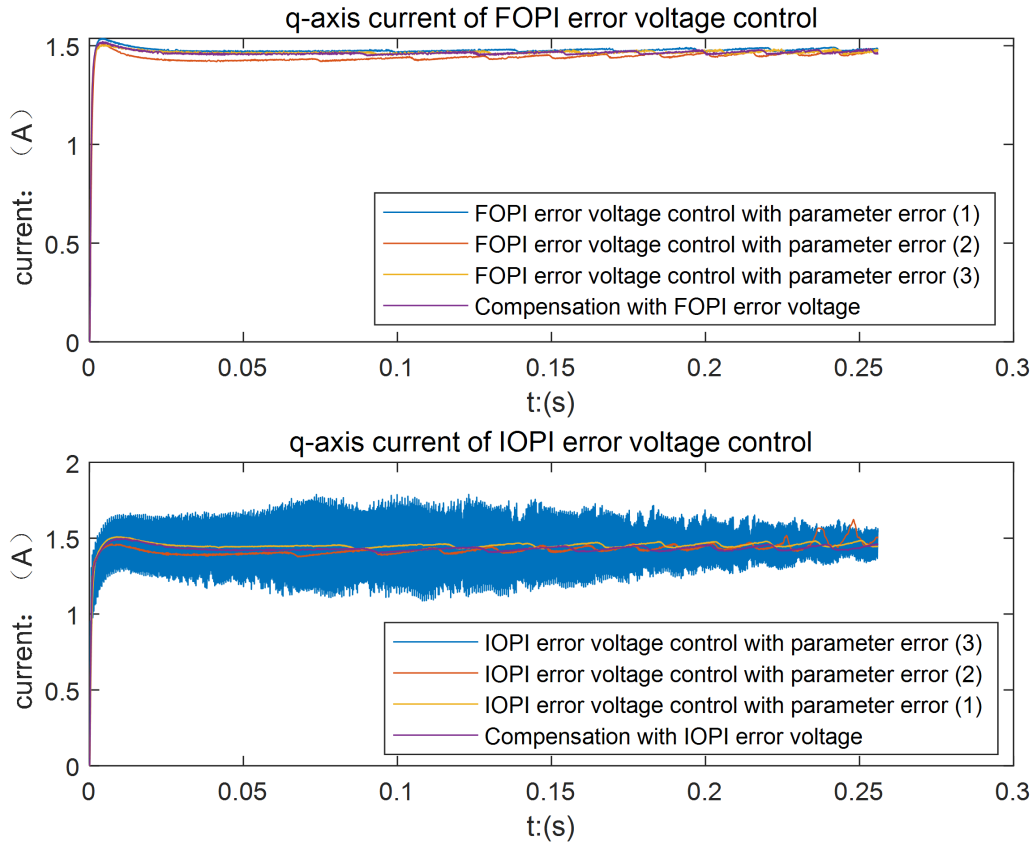

Figure 20. The comparison of I_q step current response in the error motor parameters.

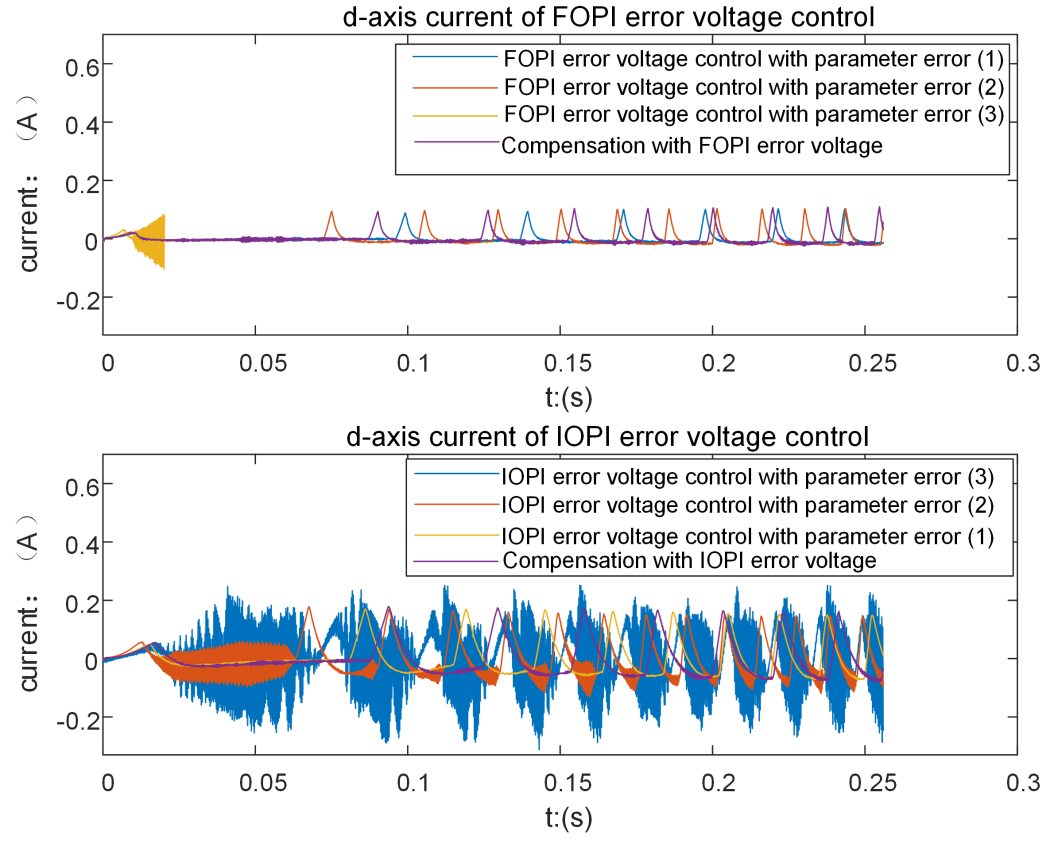

Figure 21. The comparison of I_d step current response in the error motor parameters.

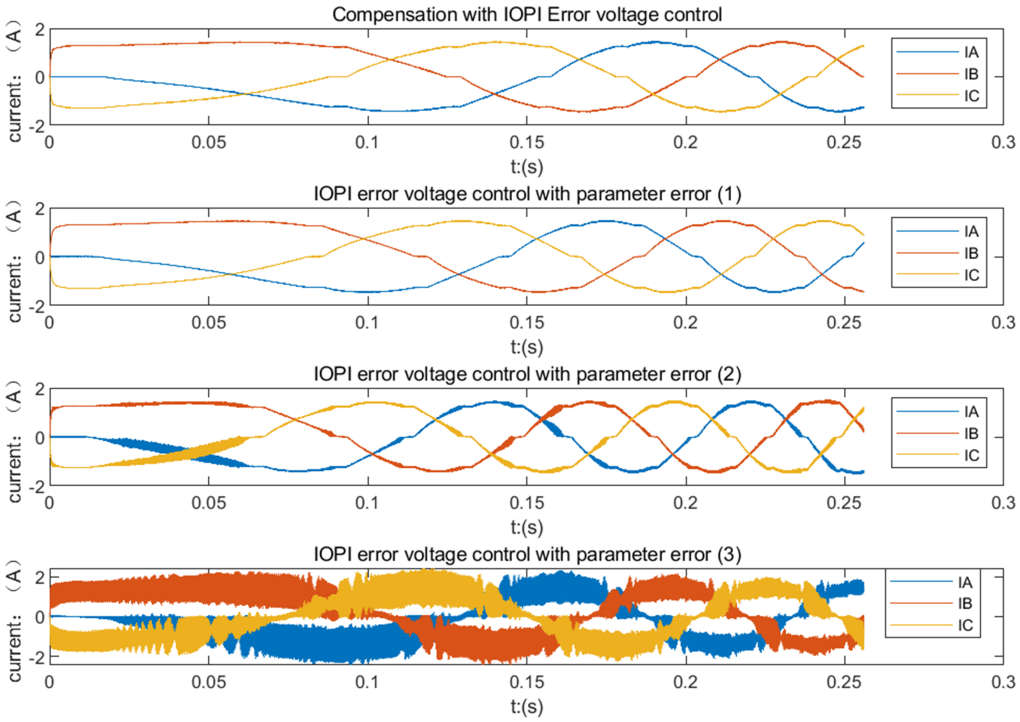

Figure 22. The three-phase current response of the optimal IOPI error voltage control in the error motor parameters.

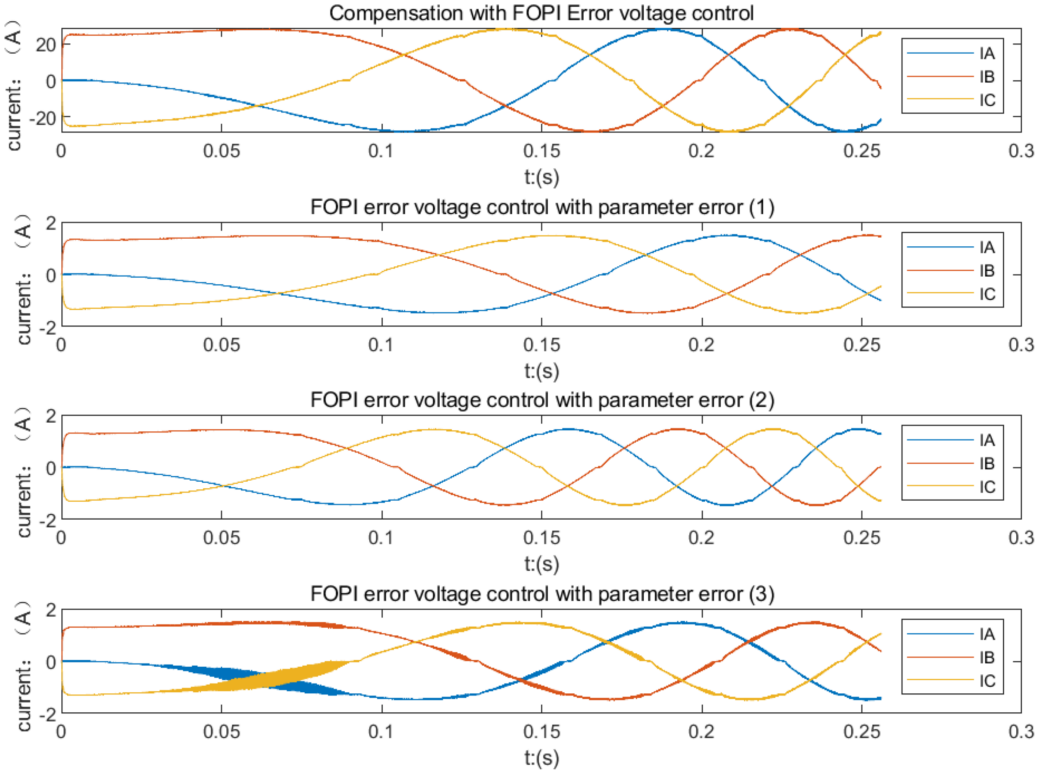

Figure 23. The three-phase current response of the optimal FOPI error voltage control in the error motor parameters.

5. Experimental Results

Experiments are performed under the same operating conditions as the simulation to demonstrate the effectiveness and high performance of the method with optimal FOPI control. A laboratory permanent magnet synchronous motor (PMSM) speed servo platform is shown in Figure 24. The experiments' dead-time setting, controller, and motor parameters are consistent with the simulation. The servo drive is based on the digital signal processor (DSP) TMS320F28335, which is used for AD conversion, encoder sampling, generation of insulated-gate bipolar transistor (IGBT) gate switching signals, and control algorithm implementation.

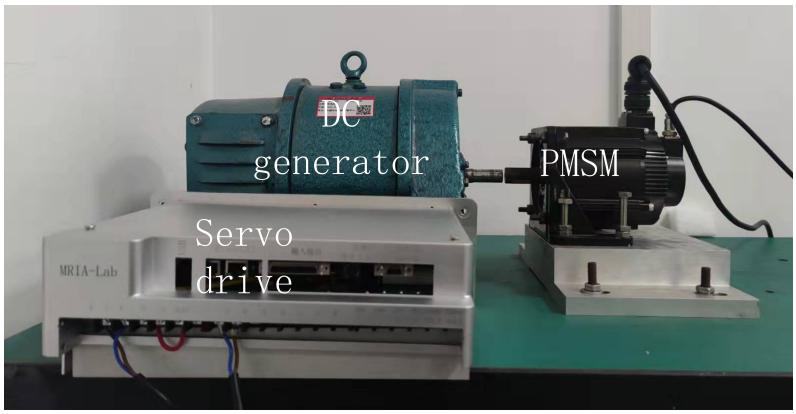

Figure 24. Experimental platform.

The experimental comparison results of the I_q current step response are shown in Figure 25 and Table 9. The I_q current step response without compensation has the characteristics of a slow rise time and large ripple. Compared with the IOPI error voltage controller and the compensation with ESO [14], it can be seen that the method with optimal FOPI error voltage control can further improve the tracking performance and reduce the current ripple of the I_q current. Compared with the compensation with ESO [14], the optimal FOPI error voltage control can effectively suppress high-frequency harmonic disturbance.

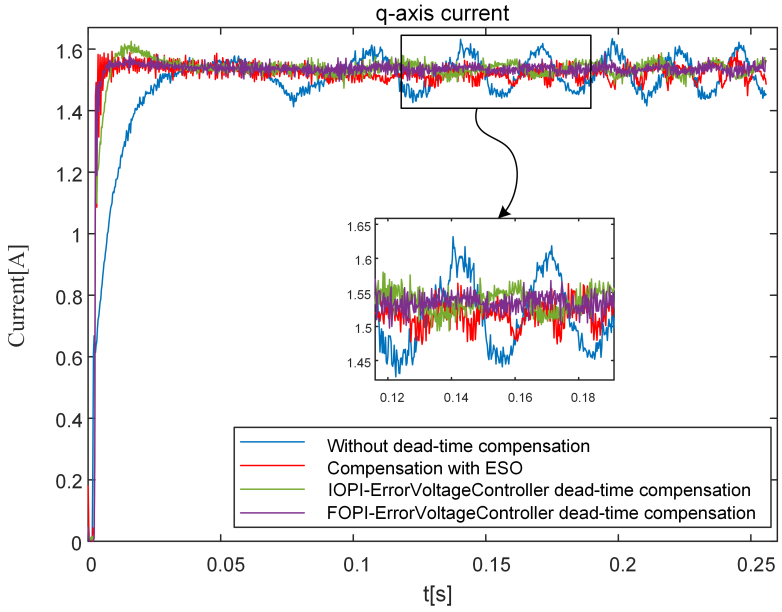

Figure 25. Comparison of I_q current response.

Table 9. The performance index comparison of I_q step current response in the experimental.

	without Compensation	IOPI	FOPI	ESO [14]
overshoot (%)	2.3	3.8	1.7	1.82
rise time (s)	0.036	0.00875	0.00675	0.00375
settling time (s)	\	0.0417	0.007	0.00376
current ripple amplitude (A)	0.1852	0.065	0.0586	0.089

In the experimental results, the I_d current response is compared under the three control strategies in Figure 26 and Table 10. Compared with the method without compensation, the dead-time compensation method with optimal IOPI error voltage control and the compensation method with ESO [14] can significantly reduce the current disturbance caused by the dead-time effect. The method with optimal FOPI error voltage control can further reduce the ripple of the I_d current than the method with optimal IOPI error voltage control and the compensation method with ESO [14].

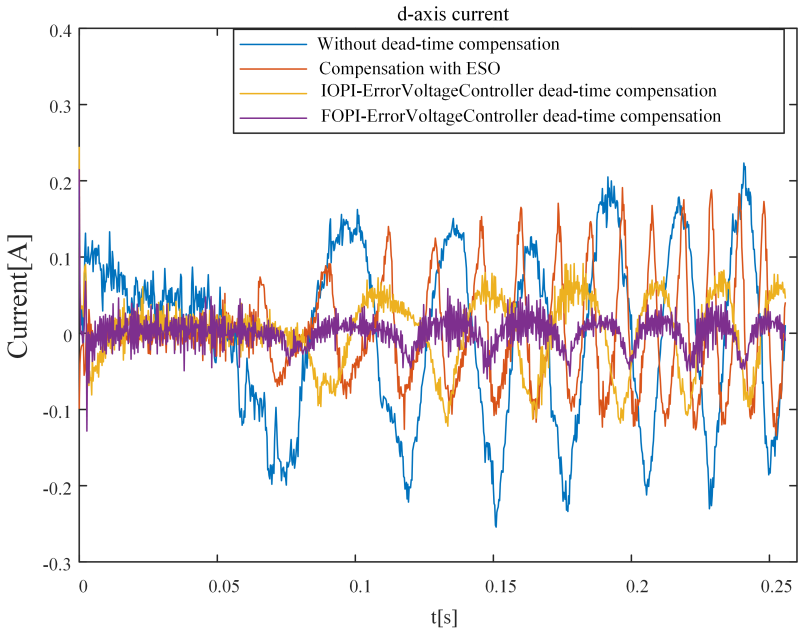

Figure 26. Comparison of I_d current response.

Table 10. The performance index comparison of I_d step current response

	without Compensation	IOPI	FOPI	ESO [14]
Current ripple amplitude (A)	0.424	0.1851	0.0732	0.291

The experimental results of the d-axis voltage error are shown in Figure 27. It can be seen that the d-axis error voltage fluctuates violently under the influence of the dead-time effect. Compared with the method without compensation and optimal IOPI error voltage control, the dead-time compensation method with optimal FOPI error voltage control can significantly reduce the d-axis error voltage.

The q-axis error voltage experimental results are shown in Figure 28. The experimental results of q-axis error voltage are consistent with the simulation results. Without compensation, the q-axis error voltage changes nonlinearly with the speed change. The error voltage can converge to 0 quickly when using the method with optimal FOPI error voltage control.

The convergence speed of the method with optimal FOPI error voltage control is faster than that using optimal IOPI error voltage control.

The above experiment studies the dead-time effect compensation effect of the method proposed in this paper in the case of current closed-loop control. Add a speed closed-loop controller to the previous current closed-loop control system, and the output of the speed closed-loop controller is used as the reference input of the current controller. When the speed is 40 r/min and 200 r/min, the experimental results of the three-phase current of the permanent magnet synchronous motor are shown in Figures 29 and 30.

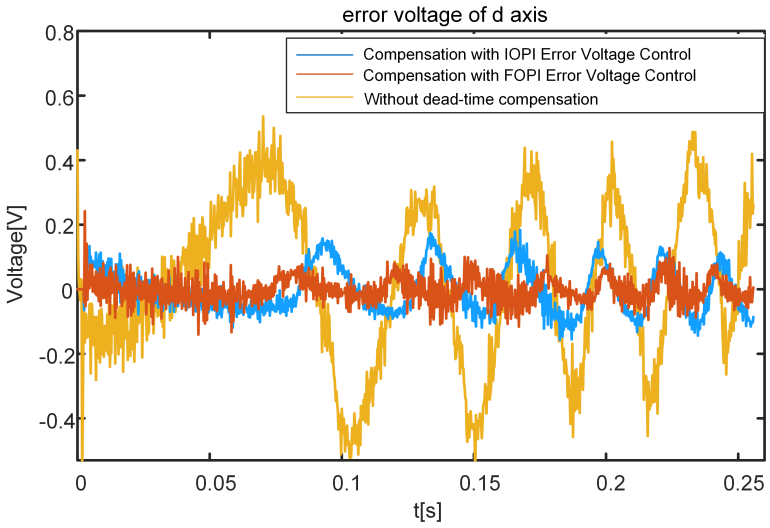

Figure 27. Comparison of the error voltage of d-axis.

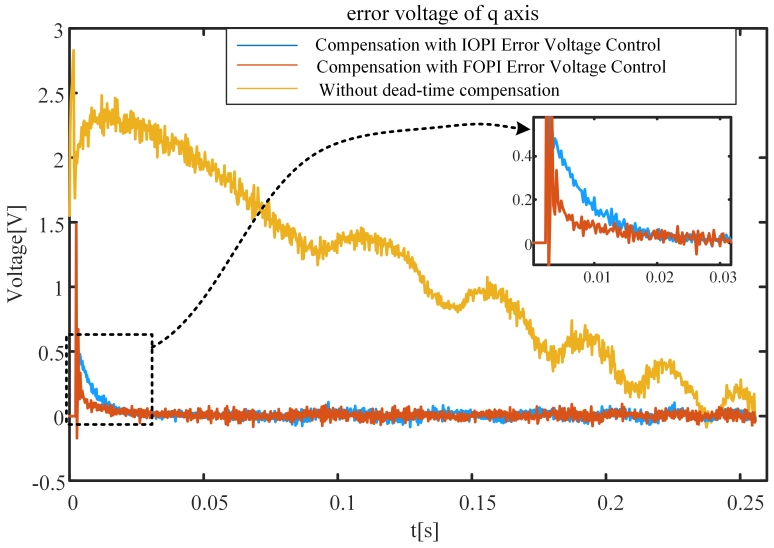

Figure 28. Comparison of the error voltage of q-axis.

The comparison of A-phase current response experimental results under the 40 r/min speed conditions is shown in Figure 29 and Table 11. Compared with the method without compensation and optimal IOPI error voltage control, the dead-time compensation method with optimal FOPI error voltage control can significantly eliminate the current distortion and reduce the clamping of current around the zero-crossing point. The three-phase current clamping time of the method proposed in this paper is less than that of the compensation method using ESO.

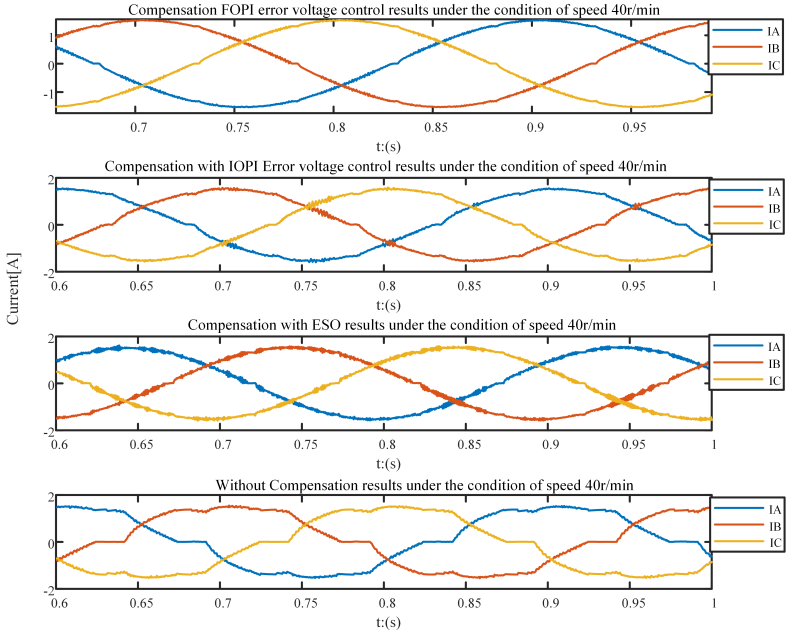

Figure 29. Comparison of Ia current response under 40 r/min speed conditions.

Table 11. The performance index comparison of I_a current step current response under 40 r/min speed conditions.

	without Compensation	IOPI	FOPI	ESO [14]
Current clamping time (s)	0.0112	0.00375	0.00175	0.00195

The comparison of A-phase current response experimental results under 200 r/min speed conditions is shown in Figures 30 and 31.

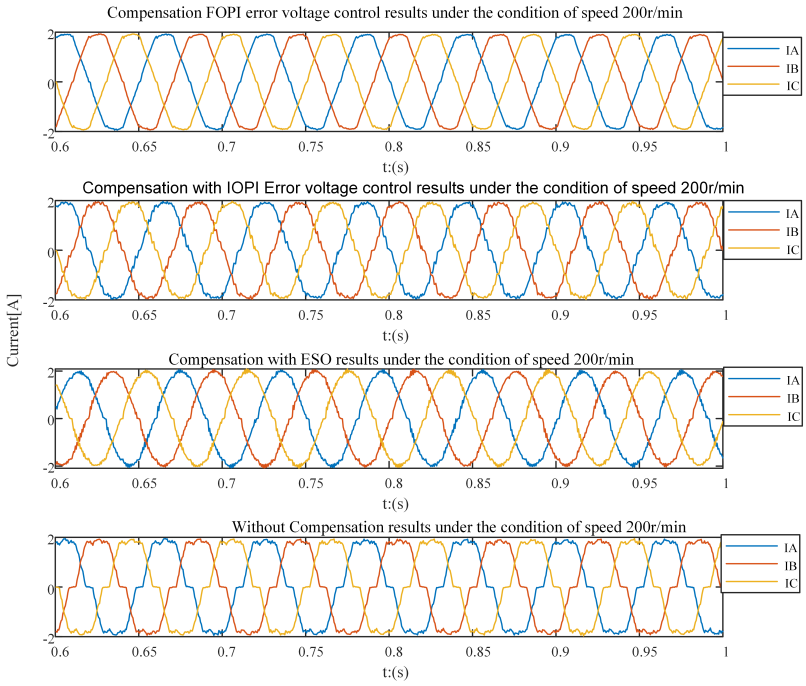

Figure 30. Comparison of three-phase current response under 200 r/min speed conditions.

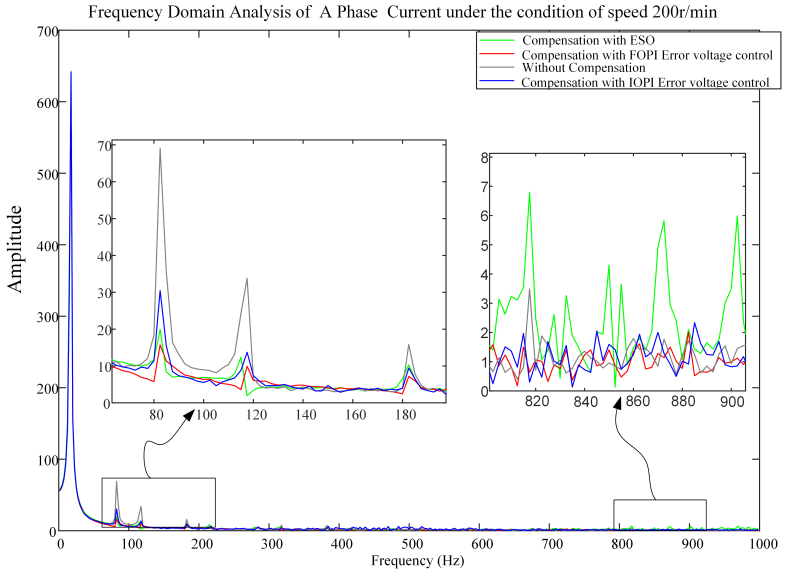

Figure 31. Frequency domain analysis of A phase current under 200 r/min speed conditions (the proposed method, the method with optimal IOPI error voltage control and the method with ESO).

In the case of keeping the motor speed constant at 200 r/min, compare the method proposed in this paper with the typical current harmonic elimination method [4]. Further, observe and compare the three-phase current and its frequency spectrum. The three-phase current experiment results and their spectrum analysis of the dead-time-related harmonic minimization method and the method [4] proposed in this paper are shown in Figures 32 and 33. It can be seen from Figure 18 that the proposed method can more effectively eliminate the current clamping phenomenon caused by the dead-time effect. At the point where the current passes through 0, the current clamping time of the proposed method is shorter than the dead-time-related harmonic minimization method [4]. It can be seen from Figure 19 that the proposed method is better than the dead-time-related harmonic minimization method [4] in eliminating the dead-time effect harmonics.

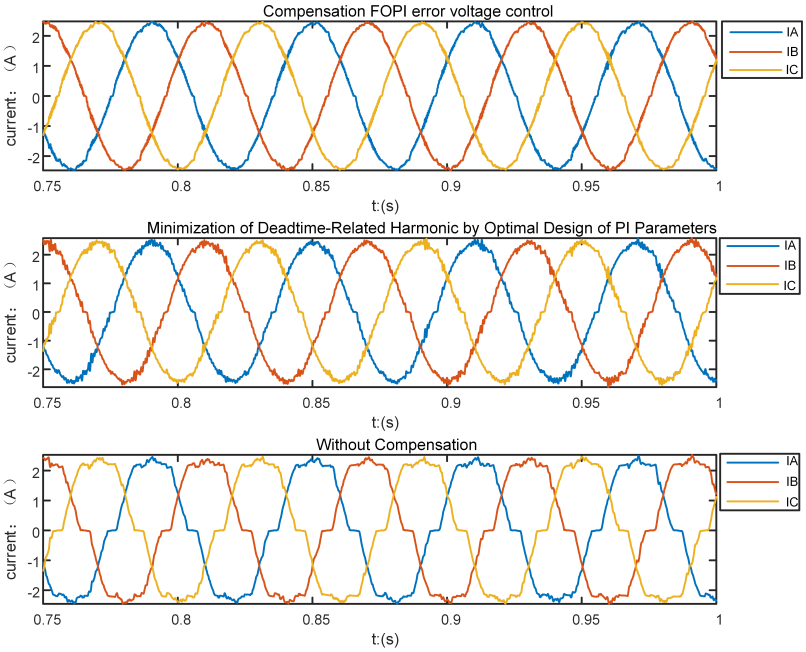

Figure 32. Comparison of three phase current respons under 200 r/min speed conditions.

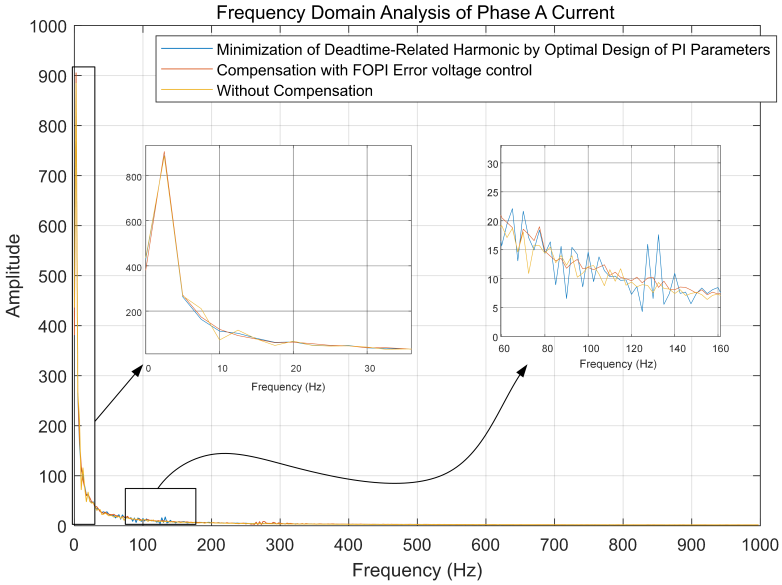

Figure 33. Frequency domain analysis of A phase current under 200 r/min speed conditions (the method with optimal IOPI error voltage control and the minimization method of deadtime-related harmonic).

6. Conclusions

This paper presents a dead-time compensation method for PMSM Servo System with optimal FOPI error voltage control. In this method, the disturbance voltages caused by the power devices' dead time and nonideal switching characteristics are compensated for by the FOPI controller and fed to the reference voltage. With the same parameter design method and parameter design index, the dead-time compensation method with optimal FOPI error voltage control is compared with the compensation method with ESO and the method with optimal IOPI error voltage control. In order to prove that the FOPI error voltage control method has a good ability to eliminate current harmonics, the dead-time-related harmonic minimization method using optimal PI parameters is compared with the proposed method. The simulation and experimental results demonstrate that the dead-time compensation method with optimal FOPI error voltage control can make the current ripple smaller and the response speed faster. Additionally, the proposed method significantly eliminates the current distortion and reduces current clamping around the zero crossing point. Through theoretical and experimental analysis, it is proven that the method proposed in this paper can have good error voltage control performance and robustness in the case of motor parameter errors. It is proven that the proposed dead-time compensation method can improve the performance of the current response by eliminating the dead-time effect.

Author Contributions: Ideas, software, validation, investigation, writing comments and editing: F.L. and Y.L. Review, commentary: X.L., P.C. and Y.C. All authors have read and agreed to the published version of the manuscript.

Funding: This work was supported by the National Natural Science Foundation of China [51975234].

Conflicts of Interest: The authors declare no conflict of interest.

References

1. Lewicki, A. Dead-time effect compensation based on additional phase current measurements. *IEEE Trans. Ind. Electron.* **2015**, *62*, 4078–4085. [CrossRef]
2. Mannen, T.; Fujita, H. Dead-Time Compensation Method Based on Current Ripple Estimation. *IEEE Trans. Power Electron.* **2015**, *30*, 4016–4024. [CrossRef]
3. Dafang, W.; Bowen, Y.; Cheng, Z.; Chuanwei, Z.; Ji, Q. A Feedback-Type Phase Voltage Compensation Strategy Based on Phase Current Reconstruction for ACIM Drives. *IEEE Trans. Power Electron.* **2014**, *29*, 5031–5043. [CrossRef]

4. Wu, Z.; Ding, K.; Yang, Z.; He, G. Analytical Prediction and Minimization of Deadtime-Related Harmonics in Permanent Magnet Synchronous Motor. *IEEE Trans. Ind. Electron.* **2020**, *68*, 7736–7746. [CrossRef]
5. Tang, Z.; Akin, B. A new LMS algorithm based deadtime compensation method for PMSM FOC drives. *IEEE Trans. Ind. Appl.* **2018**, *54*, 6472–6484. [CrossRef]
6. Qiu, T.; Wen, X.; Zhao, F. Adaptive-linear-neuron-based dead-time effects compensation scheme for PMSM drives. *IEEE Trans. Power Electron.* **2015**, *31*, 2530–2538. [CrossRef]
7. Zhu, H.; Chen, Y.; Lei, H.; Chen, D.; Li, Z. A New Dead-time Compensation Method Based on LMS Algorithm for PMSM. *J. Phys. Conf. Ser.* **2021**, *1754*, 012203. [CrossRef]
8. Liu, G.; Wang, D.; Jin, Y.; Wang, M.; Zhang, P. Current -Detection-Independent Dead-Time Compensation Method Based on Terminal Voltage A/D Conversion for PWM VSI. *IEEE Trans. Ind. Electron.* **2017**, *64*, 7689–7699. [CrossRef]
9. Su, J.H.; Hsu, B.C. Application of small-gain theorem in the dead-time compensation of voltage-source-inverter drives. *IEEE Trans. Ind. Electron.* **2005**, *52*, 1456–1458. [CrossRef]
10. Tang, N.; Brown, I.P. Framework and Solution Techniques for Suppressing Electric Machine Winding MMF Space Harmonics by Varying Slot Distribution and Coil Turns. *IEEE Trans. Magn.* **2018**, *54*, 1–12. [CrossRef]
11. Lin, C.; Xing, J.; Zhuang, X. Dead-Time Correction Applied for Extended Flux-Based Sensorless Control of Assisted PMSMs in Electric Vehicles. *Electronics* **2021**, *10*, 220. [CrossRef]
12. Miyama, Y.; Hazeyama, M.; Hanioka, S.; Watanabe, N.; Daikoku, A.; Inoue, M. PWM Carrier Harmonic Iron Loss Reduction Technique of Permanent-Magnet Motors for Electric Vehicles. *IEEE Trans. Ind. Appl.* **2016**, *52*, 2865–2871. [CrossRef]
13. Herman, L.; Papic, I.; Blazic, B. A Proportional-Resonant Current Controller for Selective Harmonic Compensation in a Hybrid Active Power Filter. *IEEE Trans. Power Deliv.* **2014**, *29*, 2055–2065. [CrossRef]
14. Shi, J.; Li, S. Analysis and compensation control of dead-time effect on space vector PWM. *J. Power Electron.* **2015**, *15*, 431–442. [CrossRef]
15. Karttunen, J.; Kallio, S.; Peltoniemi, P.; Silventoinen, P. Current Harmonic Compensation in Dual Three-Phase PMSMs Using a Disturbance Observer. *IEEE Trans. Ind. Electron.* **2016**, *63*, 583–594. [CrossRef]
16. Zhao, Y.; Qiao, W.; Wu, L. Dead-Time Effect Analysis and Compensation for a Sliding-Mode Position Observer-Based Sensorless IPMSM Control System. *IEEE Trans. Ind. Appl.* **2015**, *51*, 2528–2535. [CrossRef]
17. Guha, A.; Narayanan, G. Impact of Dead Time on Inverter Input Current, DC-Link Dynamics, and Light-Load Instability in Rectifier-Inverter-Fed Induction Motor Drives. *IEEE Trans. Ind. Appl.* **2018**, *54*, 1414–1424. [CrossRef]
18. Khurram, A.; Rehman, H.; Mukhopadhyay, S.; Ali, D. Comparative Analysis of Integer-order and Fractional-order Proportional Integral Speed Controllers for Induction Motor Drive Systems. *J. Power Electron.* **2018**, *18*, 723–735.
19. Zheng, W.; Pi, Y. Study of the fractional order proportional integral controller for the permanent magnet synchronous motor based on the differential evolution algorithm. *ISA Trans.* **2016**, *63*, 387–393. [CrossRef] [PubMed]
20. Luo, Y.; Chen, Y. Fractional order [proportional derivative] controller for a class of fractional order systems. *Automatica* **2009**, *45*, 2446–2450. [CrossRef]
21. Luo, Y.; Chen, Y.Q.; Wang, C.Y.; Pi, Y.G. Tuning fractional order proportional integral controllers for fractional order systems. *J. Process. Control.* **2010**, *20*, 823–831. [CrossRef]
22. Choi, J.W.; Sul, S.K. Inverter output voltage synthesis using novel dead time compensation. *IEEE Trans. Power Electron.* **1996**, *11*, 221–227. [CrossRef]
23. Li, Y.; Sheng, H.; Chen, Y. Impulse response invariant discretization of a generalized commensurate fractional order filter. In Proceedings of the 2010 8th World Congress on Intelligent Control and Automation, Jinan, China, 7–9 July 2010; pp. 191–196.
24. Poli, R. Analysis of the Publications on the Applications of Particle Swarm Optimisation. *J. Artif. Evol. Appl.* **2008**, *2008*, 1–10. [CrossRef]
25. Gaing, Z.L. A particle swarm optimization approach for optimum design of PID controller in AVR system. *IEEE Trans. Energy Convers.* **2004**, *19*, 384–391. [CrossRef]
26. Yoshida, H.; Kawata, K.; Fukuyama, Y.; Takayama, S.; Nakanishi, Y. A particle swarm optimization for reactive power and voltage control considering voltage security assessment. *IEEE Trans. Power Syst.* **2000**, *15*, 1232–1239. [CrossRef]
27. Karaboga, D.; Basturk, B. A powerful and efficient algorithm for numerical function optimization: Artificial bee colony (ABC) algorithm. *J. Glob. Optim.* **2007**, *39*, 459–471. [CrossRef]
28. Wang, B.; Wang, S.; Peng, Y.; Pi, Y.; Luo, Y. Design and High-Order Precision Numerical Implementation of Fractional-Order PI Controller for PMSM Speed System Based on FPGA. *Fractal Fract.* **2022**, *6*, 218. [CrossRef]